Available online at www.sciencedirect.com
SCIENCE DIRECT®
Geochimica et Cosmochimica Acta 70 (2006) 426–445
Geochimica
www.elsevier.com/locate/gca

Reassessing the uranium decay constants for geochronology using ID-TIMS U–Pb data

Blair Schoene [a,*], James L. Crowley [a], Daniel J. Condon [a], Mark D. Schmitz [b], Samuel A. Bowring [a]

[a] *Department of Earth, Atmospheric and Planetary Sciences, Massachusetts Institute of Technology, Cambridge, MA 02139, USA*
[b] *Department of Geosciences, Boise State University, Boise, ID 83725, USA*

Received 26 April 2005; accepted in revised form 12 September 2005

Abstract

As the internal precision of radiometric dates approaches the 0.1% level, systematic biases between different methods have become apparent. Many workers have suggested that calibrating other decay constants against the U–Pb system is a viable solution to this problem. We test this assertion empirically and quantitatively by analyzing U–Pb systematics of zircon and xenotime on the single- to sub-grain scale by high-precision ID-TIMS geochronology on 11 rock samples ranging from 0.1 to 3.3 Ga. Large statistically equivalent datasets give $^{207}Pb/^{206}Pb$ dates that are systematically older than $^{206}Pb/^{238}U$ dates by ~0.15% in Precambrian samples to as much as ~3.3% in Mesozoic samples, suggesting inaccuracies in the mean values of one or both of the U decay constants. These data are used to calculate a ratio of the U decay constants that is lower than the accepted ratio by 0.09% and is a factor of 5 more precise. Four of the samples are used to augment existing data from which the U–Pb and $^{40}Ar/^{39}Ar$ systems can be compared. The new data support most previous observations that U–Pb and $^{207}Pb/^{206}Pb$ dates are older than $^{40}Ar/^{39}Ar$ by $\leqslant 1\%$, though scatter in the amount of offset in samples as a function of age suggests that the bias is not entirely systematic, and may incorporate interlaboratory biases and/or geologic complexities. Studies that calibrate other decay schemes against U–Pb should include an assessment of inaccuracies in the U decay constants in addition to other systematic biases and non-systematic geologic uncertainty.

1. Introduction

Since the discovery of radioactivity and the birth of geochronology at the turn of the last century, increasingly precise dates for minerals and rocks have been used to establish a time-line for the history of the planet. In the past two decades, improvements in analytical techniques and instrument design have led to an explosion of high-precision dates using many different chronometers, such that it is now possible to explore the rates and durations of events and processes from planetary accretion to human history at the 0.1–0.2% level. However, such unparalleled precision has also revealed that systematic biases between different methods often exceed internal analytical precision, stressing the need to reevaluate the currently accepted values and associated errors for long-lived radionuclide decay constants (Begemann et al., 2001; Min et al., 2000; Renne et al., 1998a; Steiger and Jäger, 1977).

It is useful to examine this intersystem bias using the U–Pb and $^{40}Ar/^{39}Ar$ methods because they are the most widely applicable, precise, and broadly utilized geochronologic techniques, primarily due to the high concentrations of U and K in many commonly dated accessory and modal minerals, and the relatively long half-lives of the parent isotopes ($t_{1/2}$: $^{40}K \sim 1.25$ Gyr; $^{238}U \sim 4.46$ Gyr; $^{235}U \sim 0.70$ Gyr). Numerous studies (Min et al., 2000, 2001; Nomade et al., 2004; Renne, 2000; Renne et al., 1998a; Schmitz and Bowring, 2001; Villeneuve et al., 2000) have noted that $^{40}Ar/^{39}Ar$ dates are systematically younger than U–Pb dates from rapidly cooled rocks and do not overlap with U–Pb dates if one ignores systematic uncertainties. Min et al. (2000),

* Corresponding author.
E-mail address: schoene@mit.edu (B. Schoene).

0016-7037/$ - see front matter © 2005 Elsevier Inc. All rights reserved.
doi:10.1016/j.gca.2005.09.007

Renne (2000), and Renne et al. (1998a) suggest that much of the bias can be accounted for by inaccuracies in the ^{40}K decay constant and physical constants, which differ by ~2% from those used in other scientific communities. Due to the high-precision of the U decay constant measurements (0.11 and 0.14% for ^{238}U and ^{235}U, respectively; Jaffey et al., 1971) and because of the internal check of their accuracy provided by the dual decay of ^{238}U to ^{206}Pb and ^{235}U to ^{207}Pb, it has been suggested that the $^{40}Ar/^{39}Ar$ system may be calibrated against the U–Pb system (Begemann et al., 2001; Renne et al., 1998a; Villeneuve et al., 2000). Similarly, decay constants for several other lower-precision decay schemes (e.g., Lu–Hf, Re–Os, and Th–Pb) have been in part derived or tuned by comparison with U–Pb dates (e.g., Amelin and Zaitsev, 2002; Begemann et al., 2001; Chen et al., 2002; Scherer et al., 2001; Söderlund et al., 2004). Complicating this practice, however, are studies suggesting that the U decay constants of Jaffey et al. (1971) may be slightly inaccurate (though within the reported errors), based on high-precision U–Pb multi-grain zircon data from Phanerozoic samples that have $^{207}Pb/^{206}Pb$ dates that are systematically older than the $^{206}Pb/^{238}U$ dates (Mattinson, 1994a,b, 2000). Given that Pb-loss, inheritance, intermediate daughter product disequilibria, or small inaccuracies in tracer calibration could also produce this effect, it is crucial to generate additional high-precision U–Pb data in order to assess the accuracy of the U decay constants. Inaccuracies in the U decay constants not only limit the power of the U–Pb system to resolve absolute time, but also complicate high-precision intercalibration with other decay schemes.

The purpose of this contribution is to present high-precision U–Pb zircon and xenotime data from 11 rocks whose crystallization ages span over three billion years in order to (1) check for systematic internal bias in the U–Pb system by evaluating concordance of high-*n* statistically equivalent datasets and (2) to compare U–Pb results from this study and from the literature with existing $^{40}Ar/^{39}Ar$ or K–Ar data. We have purposely chosen samples in which we have resolved or eliminated the ubiquitous effects of Pb-loss and inheritance through zircon preparation methods such as the air-abrasion (Krogh, 1982) and chemical-abrasion (i.e., CA-TIMS; Mattinson, 2003, 2005) techniques, and analytical precision on single analyses is comparable to the quoted errors on the U decay constants; only such datasets provide the means to evaluate the accuracy of the U decay constants quantitatively (Mattinson, 2000; Schmitz et al., 2003). Because these samples represent over three billion years of geologic time, systematic biases in the U–Pb and $^{40}Ar/^{39}Ar$ dating techniques, which propagate as a function of age, are more readily evaluated.

2. Analytical methods

2.1. Sample preparation

Minerals were extracted from rock samples by standard crushing, Wilfley table, heavy-liquid, and magnetic separation. Fragments from large crystals and single zircons were broken into smaller fragments with a fine-tipped steel tool. Analyzed zircon was selected from the least magnetic fraction and selected based on the absence of cracks, inclusions, and surface contamination.

In order to minimize and increase the probability of concordance, zircon was subjected to one or both of the following techniques: (1) standard air-abrasion (Krogh, 1982) and total dissolution, and (2) a modified version of the chemical-abrasion technique (Mattinson, 2003, 2005). Zircon that was only air-abraded was ultrasonically cleaned in 30% HNO_3 for an hour, fluxed in 30% HNO_3 at ~80ript2O before being loaded into 300 μl Teflon FEP microcapsules and spiked with a mixed ^{233}U–^{235}U–^{205}Pb tracer. Zircon was dissolved in Parr vessels in ~120 μl of 29 M HF with ~25 μl of 30% HNO_3 at ~210 °C for 48 h, dried to fluorides, and then re-dissolved in 6 M HCl at ~180 °C overnight. For the CA-TIMS technique, zircon was placed in a muffle furnace at 900 ± 20 °C for ~60 h in quartz beakers before being transferred to 300 μl Teflon FEP microcapsules, placed in a Parr vessel, and leached in ~120 μl of 29 M HF + ~25 μl of 30% HNO_3 for 12–14 h at ~180 °C. The acid solution was removed, and fractions were rinsed in ultrapure H_2O, fluxed on a hotplate at ~80 °C for an hour in 6 M HCl, ultrasonically cleaned for an hour, and then placed back on the hotplate for an additional 30 min. The HCl solution was removed and the fractions were again rinsed in ultrapure acetone and H_2O, spiked, and fully dissolved using the procedure described above.

Xenotime was ultrasonically cleaned for an hour in H_2O, washed in 30% HNO_3 at ~50 °C for 10 min, and rinsed in ultrapure acetone and H_2O before being loaded into 300 μl Teflon FEP microcapsules and spiked with a mixed ^{233}U–^{235}U–^{205}Pb tracer. Xenotime was dissolved in 12 M HCl at ~180 °C for 48 h in a Parr vessel, dried down, and then re-dissolved in 6 M HCl at ~180 °C overnight. U and Pb for all minerals were separated using an HCl-based anion-exchange chromatographic procedure (Krogh, 1973).

2.2. Mass spectrometry and blank estimation

Most U and Pb isotopic measurements were performed on a VG Sector-54 multi-collector thermal-ionization mass spectrometer at MIT, but a few were analyzed with the Isoprobe-T multi-collector thermal-ionization mass spectrometer at MIT. Pb and U were loaded together on a single Re filament in a silica-gel/phosphoric acid mixture (Gerstenberger and Haase, 1997). Pb was measured by either peak-hopping on a single Daly detector (for smaller beams) or a dynamic Faraday–Daly routine (F–D) that cycles between placing mass 204 in the axial Daly collector and masses 205–208 on the H1–H4 Faraday detectors to placing mass 205 in the axial Daly and masses 206–208 in the H1–H3 Faradays, providing real-time Daly gain correction. U isotopic measurements were made in static Far-

aday mode or, in very low-U samples, on the Daly detector. Mass discrimination for Pb on the Daly detector was determined to be $0.25 \pm 0.04\%$/a.m.u. over a wide temperature range based on analysis of the NBS-981 common Pb standard and spiked aliquots of NBS-983. Mass fractionation and detector bias on the F–D routine was determined to be $0.07 \pm 0.04\%$/a.m.u. for the VG Sector-54 mass spectrometer and $0.09 \pm 0.04\%$/a.m.u. for the Isoprobe-T mass spectrometer based on cross-calibration with the single Daly detector runs on numerous samples and spiked aliquots of NBS-983. U mass fractionation is calculated in real time using a ^{233}U–^{235}U double spike. All common Pb for the zircon and xenotime analyses was attributed to procedural blank based on frequent total analytical blank determinations. A sensitivity test shows that the composition of the common Pb in all minerals had no effect on the calculated dates. U blanks are difficult to precisely measure, but are <0.1 pg. The $^{207}Pb/^{206}Pb$ dates are insensitive to the U blank, but variability in the U blank on low-U samples in this study can affect discordance. Therefore, a value of 0.1 pg $\pm$ 50% was used in all data reduction, and the consistency of the discordance in the results suggests this is accurate.

2.3. Tracer calibration

Improvements in analytical protocols (e.g., reduction in Pb and U blanks, improved ionization, and measurement of U isotopes as oxide species) in routine U–Pb analysis have led to the interpretation of high-*n* datasets at unprecedented precision and precipitated the recalibration of the MIT mixed ^{233}U–^{235}U–^{205}Pb tracer solution to ensure the accuracy of U–Pb dates. This recalibration was conducted from September to December of 2004. The tracer isotopic composition of U was redetermined using improved methods to control mass fractionation, including analysis as the oxide and critical mixture methods (Hofmann, 1971; Roddick et al., 1992). The isotopic composition of Pb in the tracer was determined by a combination of Daly and F–D analyses on large tracer aliquots and the same fractionation corrections made for geologic samples were used to correct these data. The calibration was carried out using standard isotope dilution methods against three mixed U–Pb gravimetric solutions prepared in independent laboratories (J. Mattinson, UCSB, pers. comm., 2004; R. Parrish, NIGL, pers. comm., 2004; and one mixed at MIT in Sept. 2004; these solutions are freely available for distribution through the EARTHTIME Network—visit www.earth-time.org). The gravimetric solutions were prepared by dissolving and quantitatively mixing different Pb and U metals of certified composition (UCSB and NIGL) and also by mixing separate Pb and U solutions of certified composition (MIT). Mass discrimination was calculated using internal U and Pb corrections (the MIT solution contained only enriched ^{206}Pb, providing no reference isotope for the internal fractionation correction. For these mixtures, the 2σ standard deviation of the fractionation determinations from the other solutions, found to be $0.12 \pm 0.03\%$/a.m.u., was used). Errors on the calibration were propagated using standard techniques, and incorporate the uncertainties in the measured isotopic ratios of calibration solutions (and the calculated Pb and U mass fractionation values) and the Pb and U isotopic compositions of the tracer and the gravimetric solutions. The standard error from a total of 11 experimental mixtures from the three gravimetric solutions was calculated in two ways: (1) by taking the weighted mean of the calculated $^{205}Pb/^{235}U$ from the 11 experiments (2SE = 0.015%; MSWD = 0.3; MSWD = mean square of the weighted deviates; York, 1966, 1967), or (2) by taking the weighted mean of the weighted means of the three solution determinations (2SE = 0.015%; MSWD = 0.2). We prefer the latter method in theory, because it would robustly account for any systematic errors arising from the weighing and mixing of the different gravimetric solutions (those errors were not propagated into the calculations because they were difficult to accurately determine for all three solutions). The low MSWDs of weighted means from these determinations suggest that systematic errors between the solutions do not exist and that we are likely overestimating one source of error. It is important to note that the new tracer composition used in this study differs from that used in previous contributions from the MIT laboratory, and the implications of this will be discussed later in the text.

2.4. Determination of reported ages and errors

Rigorous and transparent error propagation is important for intercalibrating geochronologic data between different laboratories and different methods. Quantitative discussions of error propagation and statistical analysis for the U–Pb and $^{40}Ar/^{39}Ar$ methods are presented elsewhere (Ludwig, 1980, 1998, 2000; Mattinson, 1987; Min et al., 2000; Renne et al., 1998a,b). We highlight aspects of random versus systematic errors in geochronology below. Sample-specific errors (often referred to as internal errors) are those that result from random fluctuations in the experimental conditions and define the precision of the resulting measurements. For the U–Pb method internal errors include counting statistics, uncertainties in correcting for mass discrimination, and the uncertainty in the assignment of a composition for various sources of common Pb (e.g., laboratory blank versus initial Pb in the crystal; in this study, the contribution of common Pb to the overall uncertainty is negligible). Internal errors for $^{40}Ar/^{39}Ar$ include analytical uncertainties and a variable neutron flux within an individual irradiation package. One must incorporate internal errors when testing for the equivalency of a given dataset, in turn allowing the quantitative comparison of dates relative to one another from a given laboratory.

Systematic, or "external," errors are those that affect the accuracy of measurements, and must be evaluated and applied depending on the specific situation. For example, the

uncertainties in the ages of standards used in $^{40}Ar/^{39}Ar$ geochronology only need to be incorporated when comparing dates between unknowns that use a different set of flux monitors or a different primary standard (e.g., Renne et al., 1998b). A fundamental source of systematic error in ID-TIMS geochronology is the Pb/U ratio of the mixed Pb–U tracer used in isotope dilution calculations; this source of error should be incorporated when comparing dates measured with differing isotopic spike mixtures, for example in different laboratories. Other systematic errors that are necessary when comparing data from different geochronologic methods include uncertainties in the decay constants of ^{235}U, ^{238}U, and ^{40}K, and physical constants such as the $^{40}K/K$ ratio and the branching ratio of ^{40}K (Min et al., 2000; Renne et al., 1998b).

For our purposes, it is beneficial to present data at each level of error propagation. Data reduction, age calculation, and the generation of concordia plots use the algorithms of Ludwig (1980) and/or the statistical reduction and plotting program ISOPLOT (Ludwig, 1991). For efficiency, U–Pb errors on analyses from this study are reported in the following manner, unless otherwise noted: $\pm X/Y/Z$, where X is the internal error in absence of all systematic errors, Y includes the tracer calibration error, and Z includes both tracer calibration and decay constant errors of Jaffey et al. (1971). For $^{207}Pb/^{206}Pb$ dates, tracer errors are negligible and Y is not reported (so it reads $\pm X/Z$). The MSWD (mean square of the weighted deviates; York, 1966, 1967) of equivalence refers to the probability that a weighted-mean population of isotopic ratios is statistically equivalent and is calculated prior to the addition of systematic errors (Ludwig, 1998). Concordia diagrams for the 11 samples analyzed in this study are shown in Fig. 1, data are presented in Table 1, and U–Pb dates of weighted mean clusters are summarized in Fig. 2. Errors in K–Ar and $^{40}Ar/^{39}Ar$ data considered in this paper are calculated using the methods of Karner and Renne (1998), and Renne et al. (1998b) when not provided by the original authors. All errors for U–Pb data are standard errors of the mean, unless otherwise noted, and U–Pb, K–Ar, and $^{40}Ar/^{39}Ar$ age uncertainties are presented at the 95% confidence level.

3. Sample description, previous geochronology, and U–Pb results

3.1. Narryer complex granite (JCA-62-02)

Homogeneous, weakly foliated biotite granite in the Narryer gneiss complex, northwestern Yilgarn Craton, was collected immediately north of the Jack Hills adjacent to the Sharpe Bore. Cathodoluminescence (CL) imaging shows that most zircons are dominated by concentric oscillatory zoning and some have narrow weakly zoned rims. After CL imaging, three grains that lacked obvious rims were removed from the epoxy mount, annealed, air-abraded, and broken into 10–20 fragments, some of which were chemical-abraded and analyzed. Four fragments from one grain and one fragment from another grain form a statistically significant cluster (MSWD of equivalence = 0.9). They yield a weighted mean $^{207}Pb/^{206}Pb$ date of $3313.7 \pm 0.3/7.6$ Ma (MSWD = 0.7), a weighted mean $^{207}Pb/^{235}U$ date of $3312.2 \pm 0.3/0.5/1.8$ Ma (MSWD = 0.6), and a weighted mean $^{206}Pb/^{238}U$ date of $3309.7 \pm 0.7/1.1/3.8$ Ma (MSWD = 1.1).

3.2. Kaap Valley pluton (EKC02-51)

The Kaap Valley pluton is a tonalitic multi-phase intrusion from the southeast Kaapvaal craton, southern Africa. Kamo and Davis (1994) dated six zircon and titanite fractions from two compositionally distinct phases of the pluton, giving a weighted mean $^{207}Pb/^{206}Pb$ date of 3227 ± 1 Ma (excluding systematic errors). The equivalence of titanite and zircon dates, in combination with $^{207}Pb/^{206}Pb$ apatite dates of ~3225.6 Ma (Schoene and Bowring, 2003), indicates a very rapid post-intrusion cooling history for the Kaap Valley pluton, assuming a closure temperature of ~600 °C for titanite (Cherniak, 1993; Corfu and Stone, 1998; Frost et al., 2000) and ~500 °C for apatite (Chamberlain and Bowring, 2000; Cherniak et al., 1991). Single-grain step-heating experiments on hornblende yield a weighted mean $^{40}Ar/^{39}Ar$ date of 3213.4 ± 4.3 (MSWD = 0.4; internal errors, excluding 2 of 6 analyses whose plateaus comprise <60% of total Ar released; Layer et al., 1992) relative to the primary K–Ar standard 3GR (aka Hb3gr) at 1071 Ma (Zartman, 1964).

Our sample was collected from a roadcut located several kilometers east of the pass on R61 between Badplaas and Barberton, Mpumalanga, South Africa. This phase of the pluton is a fine-grained biotite tonalite containing abundant zircon and apatite. Thirteen air-abraded zircons, one multi-grain zircon fraction, and four chemical-abraded grains were analyzed. All analyses, except for one, form a statistically significant cluster (MSWD of equivalence = 0.5). They yield a weighted mean $^{207}Pb/^{206}Pb$ date of $3227.2 \pm 0.2/7.4$ Ma (MSWD = 0.5), a weighted mean $^{207}Pb/^{235}U$ date of $3224.9 \pm 0.4/0.5/1.8$ Ma (MSWD = 0.6), and a weighted mean $^{206}Pb/^{238}U$ date of $3221.4 \pm 0.8/1.2/3.6$ Ma (MSWD = 0.5).

3.3. Eglab porphyry (EGB-032)

EGB-032 is an unmetamorphosed hornblende–biotite dacite porphyry derived from the Eglab region of the Requibath massif, west Africa (Peucat et al., 2005). Hornblende gives a weighted mean step-heating $^{40}Ar/^{39}Ar$ date of 2054.6 ± 2.4 (external sources of error excluded), based on an age of 28.02 Ma for the Fish Canyon sanidine (P. Renne, personal comm., 2005). Of 14 analyses, four air-abraded and seven chemical-abraded analyses form a single discordant cluster (MSWD of equivalence = 0.2). They yield a weighted mean $^{207}Pb/^{206}Pb$ date of $2071.6 \pm 0.4/6.1$ (MSWD = 0.2), a weighted mean $^{207}Pb/^{235}U$ date of $2069.5 \pm 0.4/0.5/1.7$ Ma (MSWD = 0.3), and a weighted

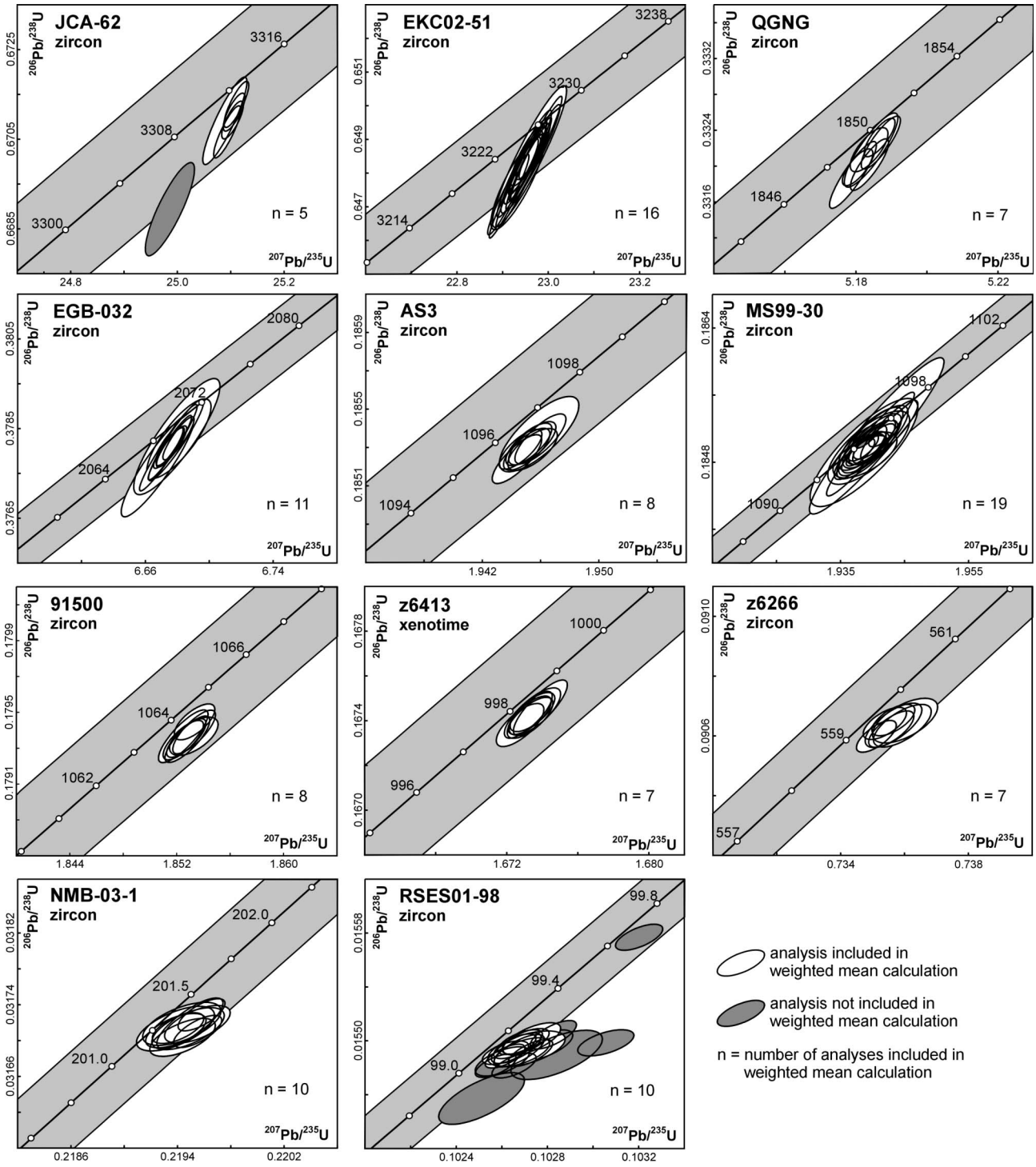

Fig. 1. U–Pb concordia diagrams. Gray band is the concordia curve error envelope using U decay constants and 95% confidence intervals from Jaffey et al. (1971). Plotted with ISOPLOT (Ludwig, 1991). Error ellipses include internal errors only and are at the 95% confidence level.

mean $^{206}Pb/^{238}U$ date of $2067.5 \pm 0.7/0.9/2.8$ (MSWD = 0.2).

3.4. QGNG

The QGNG zircon standard is derived from a quartz-gabbro/norite gneiss from the Eyre peninsula, southern Australia. Black et al. (2003b) assigned a weighted mean $^{207}Pb/^{206}Pb$ date of 1851.6 ± 0.6 Ma (MSWD = 0.6) and a weighted mean $^{206}Pb/^{238}U$ date of 1842.0 ± 3.1 Ma (both exclude decay constant errors) using a subset of the most precise, least discordant analyses that were obtained from a single laboratory. In their dataset, the $^{206}Pb/^{238}U$ dates show more variability (0.4%) than the $^{207}Pb/^{206}Pb$ dates,

Table 1
U-Pb isotopic data

Sample	$\frac{Pb^*}{Pb_c}$	Pb_c (pg)	$\frac{Th}{U}$	Isotopic ratios									Dates(Ma)						% disc.
				$\frac{^{206}Pb}{^{204}Pb}$	$\frac{^{208}Pb}{^{206}Pb}$	$\frac{^{206}Pb}{^{238}U}$	%err	$\frac{^{207}Pb}{^{235}U}$	%err	$\frac{^{207}Pb}{^{206}Pb}$	%err	corr.	$\frac{^{206}Pb}{^{238}U}$	±	$\frac{^{207}Pb}{^{235}U}$	±	$\frac{^{207}Pb}{^{206}Pb}$	±	
(a)	(b)	(c)	(d)	(e)	(f)	(f)	(g)	(f)	(g)	(f)	(g)	coef.	(h)	(i)	(h)	(i)	(h)	(i)	(j)
JCA-62-02 Granite in Narryer gneiss complex																			
z1a*	2597	0.29	0.34	139617	0.091	0.670922	0.05	25.10333	0.07	0.27137	0.04	0.787	3309.43	1.33	3312.24	0.64	3313.94	0.63	0.14
z1b*	903	0.53	0.37	48314	0.098	0.670656	0.07	25.09321	0.08	0.27137	0.04	0.863	3308.40	1.84	3311.85	0.81	3313.94	0.65	0.17
z1c*	1201	0.44	0.36	64274	0.097	0.671097	0.05	25.10611	0.07	0.27133	0.04	0.789	3310.11	1.35	3312.35	0.64	3313.71	0.63	0.11
z1d*	943	0.32	0.35	50630	0.093	0.671272	0.06	25.11060	0.08	0.27130	0.04	0.834	3310.78	1.63	3312.53	0.74	3313.58	0.65	0.08
z2a*	232	0.39	0.36	12420	0.097	0.670902	0.12	25.08919	0.13	0.27122	0.06	0.889	3309.35	3.09	3311.69	1.31	3313.11	0.96	0.11
z2b*	109	0.27	0.35	5876	0.093	0.663882	0.11	24.68440	0.13	0.26967	0.07	0.820	3282.21	2.73	3295.82	1.27	3304.10	1.17	0.66
z3*	114	0.36	0.33	6172	0.087	0.668920	0.13	24.98632	0.15	0.27091	0.08	0.850	3301.70	3.29	3307.68	1.47	3311.31	1.24	0.29
EKC02-51 Kaap Valley pluton																			
z1	66	1.79	0.54	3508	0.144	0.648392	0.16	22.96112	0.16	0.25683	0.05	0.958	3221.92	3.98	3225.30	1.60	3227.39	0.74	0.17
z5	148	0.79	0.54	7806	0.145	0.648467	0.09	22.96530	0.10	0.25685	0.05	0.871	3222.21	2.23	3225.47	0.98	3227.50	0.78	0.16
z7	53	1.06	0.46	2819	0.125	0.648074	0.16	22.94685	0.18	0.25680	0.07	0.920	3220.68	4.12	3224.69	1.72	3227.18	1.10	0.20
z8	18	1.98	0.56	959	0.149	0.648473	0.27	22.95927	0.29	0.25678	0.11	0.928	3222.24	6.74	3225.22	2.79	3227.07	1.68	0.15
z9	48	1.71	0.54	2530	0.145	0.648570	0.18	22.97234	0.19	0.25689	0.06	0.952	3222.62	4.64	3225.77	1.88	3227.73	0.93	0.16
z10	45	1.65	0.50	2399	0.135	0.644285	0.34	22.77233	0.35	0.25635	0.06	0.984	3205.84	8.58	3217.26	3.36	3224.40	0.98	0.58
z11	54	1.52	0.67	2796	0.179	0.648177	0.16	22.95640	0.17	0.25687	0.05	0.951	3221.08	4.13	3225.10	1.67	3227.60	0.83	0.20
z12	135	0.80	0.66	6953	0.176	0.648418	0.08	22.95658	0.09	0.25677	0.05	0.844	3222.02	2.03	3225.10	0.92	3227.02	0.80	0.15
z13	100	1.02	0.50	5301	0.134	0.647344	0.15	22.91348	0.16	0.25672	0.05	0.949	3217.82	3.85	3223.27	1.56	3226.67	0.80	0.27
z14	25	0.95	0.45	1356	0.120	0.648286	0.25	22.95805	0.26	0.25684	0.06	0.970	3221.51	6.34	3225.17	2.51	3227.44	1.00	0.18
z16	174	0.77	0.47	9278	0.127	0.647780	0.22	22.93461	0.22	0.25678	0.05	0.974	3219.53	5.55	3224.17	2.19	3227.06	0.80	0.23
z17	64	0.74	0.26	3571	0.070	0.648292	0.12	22.95085	0.13	0.25676	0.05	0.927	3221.53	3.08	3224.86	1.28	3226.94	0.78	0.17
z18	98	1.10	0.53	5159	0.143	0.647710	0.18	22.93388	0.21	0.25680	0.11	0.854	3219.25	4.54	3224.14	2.04	3227.18	1.73	0.25
z19a	698	1.32	0.49	37067	0.131	0.645508	0.07	22.85424	0.08	0.25678	0.04	0.867	3210.63	1.78	3220.76	0.79	3227.06	0.64	0.51
z19b	656	1.40	0.49	34848	0.131	0.645607	0.10	22.85362	0.10	0.25674	0.04	0.920	3211.02	2.41	3220.73	1.01	3226.78	0.64	0.49
za1*	83	1.28	0.34	4548	0.092	0.648511	0.12	22.95610	0.13	0.25673	0.07	0.853	3222.38	2.92	3225.08	1.31	3226.77	1.11	0.14
za3*	43	1.49	0.37	2347	0.100	0.648273	0.15	22.95005	0.17	0.25676	0.06	0.929	3221.45	3.88	3224.83	1.61	3226.92	0.96	0.17
za4*	161	1.03	0.39	8720	0.106	0.648258	0.20	22.94795	0.21	0.25674	0.07	0.951	3221.40	5.10	3224.74	2.06	3226.81	1.03	0.17
za5*	98	1.06	0.32	5405	0.086	0.648202	0.10	22.94780	0.11	0.25676	0.05	0.909	3221.17	2.55	3224.73	1.08	3226.94	0.73	0.18
EGB-032 Eglab porphyry																			
z1	50	0.56	0.68	2774	0.198	0.375949	0.22	6.63698	0.23	0.12804	0.07	0.946	2057.33	3.80	2064.28	2.02	2071.23	1.31	0.67
z2	55	0.55	0.83	2985	0.239	0.378150	0.11	6.67659	0.14	0.12805	0.08	0.841	2067.64	2.03	2069.53	1.22	2071.41	1.32	0.18
z3	62	0.61	0.51	3630	0.145	0.378797	0.12	6.70051	0.14	0.12829	0.06	0.893	2070.66	2.15	2072.69	1.20	2074.71	1.08	0.19
z4	24	0.65	0.90	1310	0.259	0.378265	0.19	6.68110	0.24	0.12810	0.15	0.801	2068.17	3.41	2070.12	2.15	2072.07	2.57	0.19
z5	23	0.72	0.75	1268	0.217	0.377682	0.25	6.66810	0.28	0.12805	0.12	0.907	2065.45	4.49	2068.40	2.49	2071.37	2.10	0.29
z8	50	0.62	0.76	2744	0.224	0.368262	0.22	6.50328	0.23	0.12808	0.08	0.942	2021.22	3.79	2046.34	2.05	2071.75	1.38	2.44
z9	16	0.47	0.77	900	0.222	0.378309	0.28	6.67986	0.33	0.12806	0.16	0.866	2068.38	4.96	2069.96	2.90	2071.55	2.90	0.15
za1*	244	0.72	0.75	13410	0.215	0.378087	0.09	6.67574	0.11	0.12806	0.05	0.870	2067.34	1.64	2069.42	0.94	2071.48	0.93	0.20
za2*	83	1.20	0.74	4596	0.212	0.378056	0.10	6.67449	0.11	0.12804	0.05	0.882	2067.20	1.76	2069.25	1.00	2071.30	0.94	0.20
za3*	143	0.58	0.55	8194	0.159	0.378089	0.10	6.67645	0.11	0.12807	0.06	0.869	2067.35	1.76	2069.51	1.01	2071.66	1.00	0.21
za4*	67	0.58	0.74	3681	0.213	0.378271	0.10	6.68083	0.12	0.12809	0.06	0.884	2068.20	1.84	2070.09	1.05	2071.96	0.97	0.18
za5*	130	0.52	0.77	7117	0.222	0.378062	0.16	6.67546	0.16	0.12806	0.05	0.949	2067.22	2.76	2069.38	1.45	2071.53	0.92	0.21
za6*	32	1.08	0.77	1768	0.221	0.378236	0.20	6.67927	0.21	0.12807	0.07	0.936	2068.04	3.49	2069.88	1.86	2071.71	1.30	0.18
za7*	80	0.51	0.79	4371	0.227	0.378060	0.21	6.67451	0.22	0.12804	0.07	0.955	2067.21	3.70	2069.25	1.94	2071.27	1.15	0.20

(*continued on next page*)

Table 1 (*continued*)

Sample	$\frac{Pb^*}{Pb_c}$	Pb_c (pg)	$\frac{Th}{U}$	Isotopic ratios									Dates(Ma)						% disc.
				$\frac{^{206}Pb}{^{204}Pb}$	$\frac{^{208}Pb}{^{206}Pb}$	$\frac{^{206}Pb}{^{238}U}$	%err	$\frac{^{207}Pb}{^{235}U}$	%err	$\frac{^{207}Pb}{^{206}Pb}$	%err	corr.	$\frac{^{206}Pb}{^{238}U}$	±	$\frac{^{207}Pb}{^{235}U}$	±	$\frac{^{207}Pb}{^{206}Pb}$	±	
(a)	(b)	(c)	(d)	(e)	(f)	(f)	(g)	(f)	(g)	(f)	(g)	coef.	(h)	(i)	(h)	(i)	(h)	(i)	(j)
QGNG																			
z1*	484	1.25	0.97	25374	0.283	0.331978	0.05	5.18061	0.07	0.11318	0.04	0.750	1847.96	0.81	1849.44	0.57	1851.10	0.81	0.17
z2*	454	0.94	1.03	23564	0.299	0.332255	0.07	5.18714	0.09	0.11323	0.05	0.845	1849.30	1.18	1850.51	0.74	1851.86	0.84	0.14
z3*	377	2.17	0.89	20179	0.258	0.332009	0.07	5.18396	0.08	0.11324	0.04	0.846	1848.11	1.14	1849.99	0.72	1852.10	0.81	0.22
z4*	256	1.83	1.00	13358	0.290	0.332171	0.10	5.18437	0.12	0.11320	0.06	0.866	1848.90	1.64	1850.05	1.01	1851.37	1.07	0.13
z5*	111	4.67	1.02	5780	0.297	0.331893	0.09	5.17929	0.10	0.11318	0.05	0.889	1847.55	1.48	1849.22	0.88	1851.10	0.86	0.19
z6.1*	759	0.47	1.00	39559	0.292	0.332313	0.05	5.18675	0.07	0.11320	0.04	0.781	1849.58	0.85	1850.44	0.58	1851.42	0.76	0.10
z7.1*	276	1.12	1.04	14305	0.303	0.332176	0.06	5.18380	0.08	0.11318	0.06	0.723	1848.92	0.98	1849.96	0.72	1851.12	1.05	0.12
AS3 Duluth Complex anorthitic series																			
za2*	330	0.89	0.61	19172	0.185	0.185287	0.05	1.94545	0.07	0.07615	0.05	0.681	1095.79	0.49	1096.88	0.48	1099.02	1.04	0.29
za4*	823	0.40	0.71	46658	0.217	0.185288	0.05	1.94505	0.07	0.07613	0.05	0.731	1095.80	0.49	1096.74	0.44	1098.60	0.90	0.26
za5*	2445	0.40	0.66	140356	0.200	0.185287	0.05	1.94462	0.06	0.07612	0.04	0.747	1095.80	0.46	1096.59	0.41	1098.18	0.82	0.22
za6*	213	1.28	0.62	12347	0.187	0.185319	0.05	1.94543	0.07	0.07614	0.05	0.734	1095.97	0.50	1096.87	0.46	1098.65	0.92	0.24
za7*	195	1.11	0.56	11487	0.169	0.185367	0.09	1.94590	0.11	0.07614	0.07	0.763	1096.23	0.88	1097.03	0.77	1098.65	1.48	0.22
za8*	775	0.76	0.65	44570	0.198	0.185342	0.06	1.94598	0.07	0.07615	0.05	0.788	1096.09	0.58	1097.06	0.49	1098.98	0.90	0.26
za9*	635	0.91	0.61	36929	0.185	0.185313	0.05	1.94519	0.07	0.07613	0.04	0.743	1095.94	0.49	1096.79	0.44	1098.51	0.89	0.23
za10*	987	0.74	0.62	57263	0.187	0.185236	0.06	1.94438	0.07	0.07613	0.04	0.797	1095.52	0.57	1096.51	0.47	1098.51	0.85	0.27
MS99-30 Palisade rhyolite																			
za2*	100	0.96	0.83	5545	0.252	0.184970	0.07	1.93859	0.10	0.07601	0.07	0.735	1094.07	0.72	1094.51	0.65	1095.40	0.72	0.12
za3*	79	1.25	0.89	4295	0.270	0.184947	0.16	1.93919	0.20	0.07605	0.12	0.791	1093.94	1.58	1094.72	1.33	1096.25	1.33	0.21
za4*	48	0.92	0.89	2609	0.269	0.185036	0.11	1.94024	0.14	0.07605	0.08	0.806	1094.43	1.13	1095.08	0.94	1096.37	0.91	0.18
za6*	36	1.20	0.81	2029	0.245	0.184909	0.14	1.93815	0.17	0.07602	0.09	0.837	1093.74	1.43	1094.36	1.15	1095.63	1.03	0.17
za7*	26	4.91	0.85	1435	0.259	0.185003	0.16	1.93958	0.21	0.07604	0.12	0.804	1094.25	1.65	1094.85	1.37	1096.07	1.34	0.17
za10*	204	1.15	0.82	11341	0.250	0.184910	0.07	1.93813	0.09	0.07602	0.06	0.775	1093.74	0.73	1094.35	0.63	1095.58	0.65	0.17
z1	43	3.69	0.78	2396	0.240	0.183121	0.10	1.92213	0.13	0.07613	0.08	0.779	1084.00	1.02	1088.81	0.88	1098.42	0.90	1.31
z1.1	34	0.90	0.68	1948	0.207	0.184877	0.12	1.93883	0.21	0.07606	0.16	0.634	1093.56	1.22	1094.59	1.40	1096.65	1.78	0.28
z2	19	3.32	0.89	1035	0.269	0.184966	0.19	1.93941	0.27	0.07605	0.18	0.743	1094.05	1.95	1094.80	1.79	1096.28	1.96	0.20
z2.1	59	0.94	0.76	3323	0.231	0.184958	0.09	1.93930	0.14	0.07605	0.11	0.650	1094.00	0.86	1094.76	0.93	1096.28	1.16	0.21
z3	77	1.51	0.85	4257	0.259	0.184996	0.07	1.93955	0.11	0.07604	0.08	0.698	1094.21	0.73	1094.84	0.72	1096.09	0.84	0.17
z4	61	1.20	0.88	3340	0.266	0.185009	0.27	1.93968	0.29	0.07604	0.08	0.955	1094.28	2.76	1094.89	1.92	1096.09	0.93	0.16
z4.1	55	1.37	0.83	3044	0.253	0.184936	0.08	1.93934	0.13	0.07606	0.10	0.620	1093.89	0.77	1094.77	0.86	1096.56	1.10	0.24
z5	23	2.52	0.84	1286	0.254	0.185072	0.17	1.93971	0.21	0.07601	0.13	0.790	1094.62	1.68	1094.90	1.42	1095.44	1.42	0.07
z5.1	27	1.27	0.86	1485	0.262	0.185096	0.17	1.94045	0.21	0.07603	0.13	0.788	1094.76	1.67	1095.16	1.43	1095.95	1.44	0.11
z6.1	37	1.87	0.87	2036	0.265	0.184898	0.10	1.93856	0.14	0.07604	0.10	0.734	1093.68	1.03	1094.50	0.94	1096.14	1.04	0.22
z6	115	1.49	0.77	6421	0.236	0.182514	0.05	1.91220	0.08	0.07599	0.06	0.658	1080.70	0.53	1085.35	0.55	1094.69	0.68	1.28
z7	98	11.89	0.78	5407	0.236	0.185114	0.06	1.94145	0.09	0.07606	0.06	0.713	1094.85	0.61	1095.50	0.58	1096.79	0.66	0.18
z9	14	4.05	0.79	818	0.239	0.184908	0.29	1.93870	0.35	0.07604	0.20	0.816	1093.73	2.87	1094.55	2.37	1096.18	2.24	0.22
z10	39	1.70	0.82	2174	0.250	0.185107	0.41	1.94068	0.44	0.07604	0.15	0.944	1094.82	4.16	1095.23	2.95	1096.04	1.59	0.11
z11	36	2.03	0.85	1978	0.258	0.185173	0.16	1.94262	0.19	0.07609	0.09	0.862	1095.17	1.62	1095.90	1.25	1097.35	1.04	0.20
91500																			
z2	227	2.47	0.36	14093	0.108	0.179343	0.05	1.85250	0.07	0.07492	0.04	0.760	1063.38	0.49	1064.32	0.44	1066.26	0.87	0.27
z12	1654	0.96	0.35	102639	0.106	0.179348	0.06	1.85281	0.07	0.07493	0.04	0.805	1063.41	0.58	1064.43	0.48	1066.53	0.87	0.29
z13	1058	0.84	0.36	65582	0.108	0.179354	0.05	1.85272	0.06	0.07492	0.04	0.764	1063.44	0.48	1064.40	0.42	1066.39	0.84	0.28
z14	1073	0.83	0.35	66606	0.107	0.179364	0.07	1.85251	0.08	0.07491	0.05	0.828	1063.50	0.66	1064.32	0.54	1066.02	0.92	0.24

z15	389	1.72	0.34	24213	0.105	0.179388	0.06	1.85331	0.07	0.07493	0.04	0.789	1063.63	0.54	1064.61	0.46	1066.62	0.87	0.28
z18	372	0.61	0.35	23079	0.107	0.179444	0.05	1.85335	0.07	0.07491	0.05	0.688	1063.94	0.45	1064.62	0.44	1066.02	0.97	0.20
z20	210	0.87	0.35	13016	0.107	0.179364	0.05	1.85330	0.08	0.07494	0.06	0.615	1063.50	0.48	1064.60	0.52	1066.85	1.26	0.31
z6413																			
x1k	11286	0.49	0.16	738065	0.049	0.167425	0.05	1.67321	0.07	0.07248	0.04	0.789	997.91	0.48	998.41	0.42	999.50	0.82	0.16
x1m	5476	0.30	0.15	359189	0.045	0.167455	0.06	1.67389	0.07	0.07250	0.04	0.826	998.08	0.56	998.66	0.47	999.95	0.85	0.19
x1n	5158	0.13	0.17	336515	0.050	0.167439	0.05	1.67358	0.07	0.07249	0.05	0.736	997.99	0.48	998.55	0.45	999.77	0.97	0.18
x1p	4623	0.16	0.17	301712	0.050	0.167422	0.04	1.67329	0.06	0.07249	0.04	0.716	997.89	0.39	998.44	0.37	999.63	0.83	0.17
x1q	2622	0.21	0.17	171135	0.051	0.167379	0.05	1.67275	0.07	0.07248	0.05	0.723	997.65	0.44	998.23	0.42	999.50	0.92	0.18
x1r	2478	0.23	0.17	161766	0.051	0.167410	0.04	1.67331	0.06	0.07249	0.04	0.716	997.83	0.42	998.44	0.40	999.82	0.89	0.20
x1u	2494	0.21	0.16	162828	0.050	0.167436	0.04	1.67344	0.06	0.07249	0.04	0.702	997.97	0.40	998.49	0.39	999.63	0.88	0.17
z6266																			
z1	88	0.62	0.22	5736	0.068	0.090650	0.07	0.73602	0.11	0.05889	0.09	0.610	559.38	0.36	560.08	0.48	562.91	1.94	0.63
z3	83	2.02	0.22	5426	0.069	0.090634	0.07	0.73566	0.10	0.05887	0.07	0.698	559.28	0.36	559.87	0.42	562.24	1.54	0.52
z7a*	165	0.55	0.22	10733	0.069	0.090652	0.05	0.73565	0.07	0.05886	0.06	0.639	559.39	0.25	559.86	0.32	561.76	1.25	0.42
z9a*	105	0.71	0.22	6821	0.069	0.090621	0.05	0.73559	0.08	0.05887	0.06	0.707	559.21	0.29	559.83	0.34	562.37	1.21	0.56
z10a*	76	0.72	0.22	4972	0.069	0.090633	0.06	0.73593	0.10	0.05889	0.07	0.667	559.28	0.34	560.03	0.43	563.12	1.63	0.68
z12a*	288	0.39	0.22	18719	0.069	0.090641	0.05	0.73539	0.08	0.05884	0.06	0.648	559.32	0.26	559.71	0.32	561.31	1.25	0.35
z13a*	263	0.67	0.22	17098	0.069	0.090597	0.05	0.73512	0.07	0.05885	0.05	0.701	559.07	0.26	559.56	0.30	561.52	1.07	0.44
NMB-03-1 N North Mountain basalt																			
z3	156	1.10	2.23	6468	0.720	0.031713	0.06	0.21948	0.10	0.05020	0.08	0.625	201.26	0.12	201.48	0.18	204.10	1.83	1.39
z4	195	1.13	2.00	8459	0.642	0.031711	0.05	0.21939	0.08	0.05018	0.07	0.596	201.25	0.10	201.40	0.15	203.22	1.57	0.97
z5	131	0.77	1.63	6078	0.526	0.031718	0.05	0.21955	0.09	0.05020	0.07	0.607	201.29	0.11	201.54	0.17	204.47	1.68	1.55
z8	187	0.56	2.23	7788	0.714	0.031713	0.06	0.21939	0.11	0.05017	0.09	0.618	201.26	0.13	201.40	0.20	203.08	1.98	0.89
z11	155	0.92	1.85	6899	0.596	0.031703	0.05	0.21944	0.09	0.05020	0.07	0.618	201.20	0.11	201.45	0.17	204.32	1.67	1.53
z12	136	0.80	2.29	5612	0.733	0.031718	0.06	0.21944	0.11	0.05018	0.09	0.597	201.29	0.12	201.44	0.20	203.22	2.03	0.95
z18	1658	0.44	2.50	65403	0.804	0.031728	0.05	0.21959	0.07	0.05019	0.05	0.712	201.36	0.09	201.56	0.12	204.03	1.07	1.31
z19	1967	0.38	2.36	79326	0.764	0.031710	0.05	0.21956	0.07	0.05022	0.05	0.696	201.24	0.09	201.54	0.12	205.05	1.11	1.86
z20	283	1.34	1.86	12607	0.597	0.031719	0.07	0.21950	0.09	0.05019	0.06	0.796	201.30	0.14	201.49	0.17	203.81	1.29	1.23
z21	345	1.41	2.42	13836	0.776	0.031713	0.04	0.21941	0.07	0.05018	0.06	0.624	201.26	0.09	201.42	0.13	203.22	1.30	0.96
RSES01-98 (GA-1550)																			
z1	185	1.22	0.38	11716	0.121	0.015496	0.05	0.10266	0.07	0.04805	0.05	0.669	99.12	0.05	99.23	0.07	101.72	1.29	2.55
z2	205	0.64	0.70	11944	0.222	0.015499	0.05	0.10268	0.08	0.04805	0.06	0.640	99.14	0.05	99.25	0.07	101.80	1.40	2.61
z3	72	0.85	0.34	4645	0.109	0.015501	0.06	0.10273	0.10	0.04807	0.08	0.649	99.16	0.06	99.30	0.10	102.62	1.81	3.37
z4	154	0.83	0.67	9017	0.215	0.015499	0.05	0.10271	0.08	0.04806	0.06	0.633	99.15	0.05	99.27	0.08	102.24	1.50	3.03
z5	106	1.25	0.50	6530	0.159	0.015484	0.06	0.10261	0.09	0.04806	0.07	0.621	99.05	0.06	99.18	0.09	102.24	1.75	3.12
z6	298	0.99	0.56	17994	0.178	0.015577	0.05	0.10320	0.08	0.04805	0.06	0.633	99.64	0.05	99.73	0.08	101.79	1.49	2.12
z7	447	1.02	0.46	27591	0.148	0.015488	0.05	0.10262	0.07	0.04805	0.05	0.680	99.08	0.05	99.19	0.07	101.87	1.20	2.74
z9	154	0.71	0.45	9523	0.145	0.015491	0.05	0.10262	0.08	0.04805	0.06	0.599	99.09	0.05	99.19	0.08	101.50	1.52	2.37
z10	103	0.50	0.65	6051	0.209	0.015498	0.05	0.10306	0.10	0.04823	0.08	0.569	99.14	0.05	99.59	0.09	110.47	1.88	10.25
z10.5	332	0.94	0.76	19001	0.245	0.015504	0.06	0.10283	0.08	0.04810	0.06	0.697	99.18	0.05	99.38	0.08	104.34	1.36	4.94
z11	326	0.93	0.63	19253	0.203	0.015491	0.05	0.10273	0.08	0.04810	0.06	0.693	90.09	0.05	99.29	0.07	104.04	1.32	4.75
z12	96	1.17	0.49	5911	0.158	0.015496	0.06	0.10279	0.09	0.04811	0.07	0.648	99.13	0.06	99.35	0.09	104.71	1.71	5.33
z13	98	2.64	0.52	5955	0.166	0.015494	0.06	0.10267	0.09	0.04806	0.06	0.704	99.12	0.06	99.23	0.08	102.09	1.45	2.92
z15	173	0.92	0.79	9822	0.254	0.015481	0.05	0.10258	0.07	0.04806	0.05	0.654	99.03	0.05	99.15	0.07	102.02	1.27	2.93
z16	35	3.93	0.47	2174	0.151	0.015489	0.10	0.10284	0.16	0.04816	0.12	0.637	99.08	0.10	99.40	0.15	106.88	2.89	7.29
z17aa	55	1.33	0.58	3317	0.187	0.015456	0.10	0.10252	0.15	0.04810	0.11	0.697	98.88	0.10	99.10	0.14	104.34	2.53	5.23
z18aa	137	1.27	0.53	8328	0.171	0.015481	0.05	0.10266	0.08	0.04809	0.06	0.639	99.03	0.05	99.23	0.07	103.89	1.40	4.67

(*continued on next page*)

Table 1 (*continued*)

Sample	$\frac{Pb^*}{Pb_c}$	Pb_c (pg)	$\frac{Th}{U}$	Isotopic ratios								Dates(Ma)						% disc.
				$\frac{^{206}Pb}{^{204}Pb}$	$\frac{^{208}Pb}{^{206}Pb}$	$\frac{^{206}Pb}{^{238}U}$	%err	$\frac{^{207}Pb}{^{235}U}$	%err	$\frac{^{207}Pb}{^{206}Pb}$	%err	corr.	$\frac{^{206}Pb}{^{238}U}$	±	$\frac{^{207}Pb}{^{235}U}$	±	$\frac{^{207}Pb}{^{206}Pb}$	±	
(a)	(b)	(c)	(d)	(e)	(f)	(f)	(g)	(f)	(g)	(f)	(g)	coef.	(h)	(i)	(h)	(i)	(h)	(i)	(j)
z21a*	65	0.71	0.57	3923	0.182	0.015494	0.07	0.10271	0.13	0.04808	0.11	0.547	99.11	0.07	99.28	0.13	103.22	2.66	3.98
z23a*	84	0.61	0.46	5177	0.148	0.015491	0.06	0.10269	0.10	0.04808	0.08	0.601	99.10	0.06	99.26	0.09	103.14	1.82	3.92
z24a*	195	1.02	0.59	11667	0.190	0.015492	0.06	0.10268	0.09	0.04807	0.06	0.725	99.10	0.06	99.25	0.08	102.69	1.44	3.49

(a) z1, z2 etc. are labels for fractions composed of single grains or fragments of grains; x = xenotime, z = zircon; * denotes zircon fractions that were subjected to the chemical abrasion technique (all others, except the xenotime, underwent mechanical abrasion); Labels with bold text denote fractions used in the weighted mean calculations (see text and Fig. 2).
(b) Ratio of radiogenic Pb to common Pb.
(c) Total weight of common Pb.
(d) Model Th/U ratio calculated from radiogenic 208Pb/206Pb ratio and 207Pb/206Pb age.
(e) Measured ratio corrected for spike and fractionation only. Mass fractionation corrections were based on analysis of NBS-981 and NBS-983. Corrections of 0.25 ± 0.04%/amu (atomic mass unit) and 0.07 ± 0.04%/amu were applied to single-collector Daly analyses and dynamic Faraday-Daly analyses, respectively, performed on the Sector-54 mass spectrometer. Correction of 0.09 ± 0.04%/amu was applied to dynamic Faraday-Daly analyses performed on the Isoprobe-T mass spectrometer.
(f) Corrected for fractionation, spike, blank, and initial common Pb. All common Pb was assumed to be procedural blank.
(g) Errors are 2 sigma, propagated using the algorithms of Ludwig (1980).
(h) Calculations are based on the decay constants of Jaffey et al. (1971).
(i) Errors are 2 sigma.
(j) % discordance = 100 − (100 × 206Pb/238U date/207Pb/206Pb date).

and the $^{206}Pb/^{238}U$ date was taken as the most reliable value based on the inference that the volumetrically dominant interior parts of the grains had lost ~0.5% of their radiogenic Pb. Our dataset includes seven chemical-abraded grains that form a discordant cluster (MSWD of equivalence = 1.5). They yield a weighted mean $^{207}Pb/^{206}Pb$ date of 1851.5 ± 0.3/5.8 Ma (MSWD = 1.2), a weighted mean $^{207}Pb/^{235}U$ date of 1850.0 ± 0.5/0.6/1.7 Ma (MSWD = 1.9), and a weighted mean $^{206}Pb/^{238}U$ date of 1848.7 ± 0.7/0.9/2.7 Ma (MSWD = 2.1).

3.5. Duluth Complex anorthositic series (AS3)

AS3 is from the Duluth Complex anorthositic series, northern Minnesota, USA (Paces and Miller, 1993; Schmitz et al., 2003). Schmitz et al. (2003) assigned a U–Pb concordia age of 1099.1 ± 0.2 Ma (±1.2 Ma including tracer calibration and decay constant errors) using a subset of concordant analyses, which agrees with a $^{207}Pb/^{206}Pb$ date of 1099.1 ± 0.5/5.0 Ma (without/with decay constant errors) obtained by Paces and Miller (1993). Eight grains from the same population utilized by Schmitz and Bowring (2001) were chemical-abraded and the results form a statistically significant discordant cluster (MSWD of equivalence = 0.4). They yield a weighted mean $^{207}Pb/^{206}Pb$ date of 1098.6 ± 0.3/5.0 Ma (MSWD = 0.4), a weighted mean $^{207}Pb/^{235}U$ date of 1096.8 ± 0.2/0.3/1.2 Ma (MSWD = 0.6), and a weighted mean $^{206}Pb/^{238}U$ date of 1095.9 ± 0.2/0.3/1.4 Ma (MSWD = 0.5).

3.6. Palisade rhyolite (MS99-30)

The Palisade rhyolite is part of the North Shore Volcanic group, associated with the failed Mesoproterozoic Midcontinent rift of central North America (Davis and Green, 1997; Green, 1977; Green et al., 1993). Min et al. (2000) reported nine concordant single-grain sanidine incremental heating experiments that gave a weighted mean $^{40}Ar/^{39}Ar$ date of 1088.4 ± 4.0 Ma (internal errors only) relative to an age of 28.02 Ma for the Fish Canyon sanidine, which they interpreted as the eruption age for the Palisade rhyolite. They also augmented a previous discordant zircon dataset (Davis and Green, 1997) by reporting a weighted mean $^{207}Pb/^{206}Pb$ date of 1097.6 ± 2.1 Ma (external errors excluded) for the 14 analyses from both datasets.

Densely welded rhyolite was collected from a roadcut near the junction of highways 61 and 1, a few kilometers north of Palisade Head, Minnesota. Twenty-one zircon grains were analyzed including 15 air-abraded grains and six chemical-abraded grains. Nineteen analyses define a single discordant cluster (MSWD of equivalence = 0.5). They yield a weighted mean $^{207}Pb/^{206}Pb$ date of 1096.1 ± 0.4/5.0 (MSWD = 0.3), a weighted mean $^{207}Pb/^{235}U$ date of 1094.8 ± 0.2/0.3/1.2 (MSWD = 0.8), and a weighted mean $^{206}Pb/^{238}U$ date of 1094.2 ± 0.2/0.4/1.5 Ma (MSWD = 0.7).

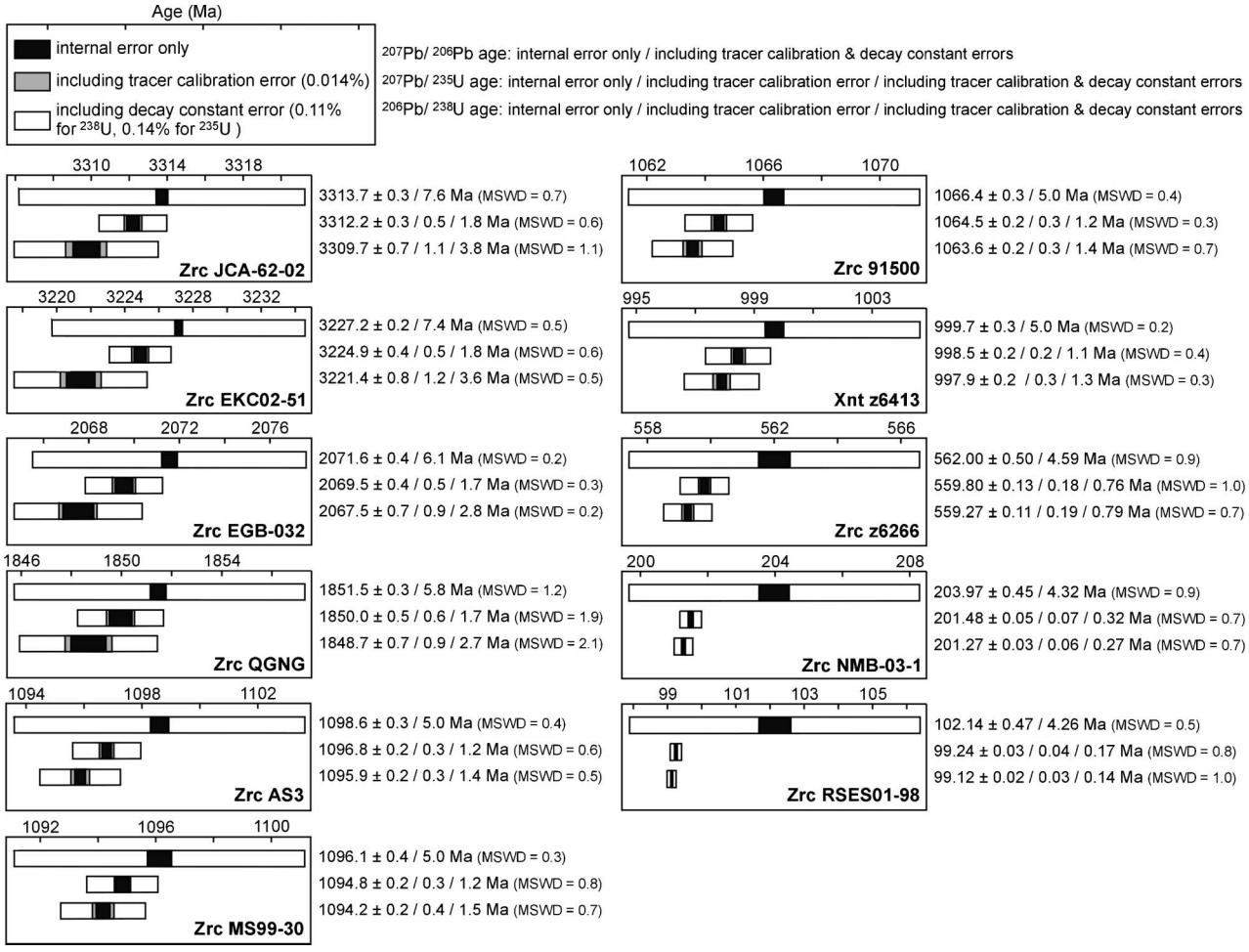

Fig. 2. Weighted mean U–Pb dates (in Ma) for equivalent data clusters. Analyses included in the weighted mean calculations are shown in Table 1 and Fig. 1. Errors are at the 95% confidence level.

3.7. Zircon 91500

Zircon crystal 91500 is from a syenite pegmatite in Ontario, Canada (Hewitt, 1953; Wiedenbeck et al., 1995). Wiedenbeck et al. (1995) assigned a weighted mean $^{207}Pb/^{206}Pb$ date of 1065.4 ± 0.6 Ma (MSWD = 1.3) and a weighted mean $^{206}Pb/^{238}U$ date of 1062.4 ± 0.8 Ma (MSWD = 2.1) based on data from three laboratories. Similar $^{207}Pb/^{206}Pb$ dates were more recently reported, but some of the analyses are more discordant (Amelin and Zaitsev, 2002; Paquette and Pin, 2001). Large fragments that we obtained were broken and air-abraded. Seven fragments form a statistically significant cluster (MSWD of equivalence = 0.5). They yield a weighted mean $^{207}Pb/^{206}Pb$ date of $1066.4 \pm 0.3/5.0$ Ma (MSWD = 0.4), a weighted mean $^{207}Pb/^{235}U$ date of $1064.5 \pm 0.2/0.3/1.2$ Ma (MSWD = 0.3), and a weighted mean $^{206}Pb/^{238}U$ date of $1063.6 \pm 0.2/0.3/1.4$ Ma (MSWD = 0.7).

3.8. Xenotime z6413

z6413 is derived from a granite which contains megacrysts of xenotime, originally collected from within the Purdy #3 Mine, Mattawan Township, Ontario, Canada (see Stern and Rayner, 2003 for detailed description). Stern and Rayner (2003) assigned a weighted mean $^{207}Pb/^{206}Pb$ date of 996.7 ± 0.8 Ma (MSWD = 0.7) and a weighted mean $^{206}Pb/^{238}U$ date of 993.8 ± 0.7 Ma (MSWD = 0.3). Seven small fragments that we analyzed form a statistically significant cluster (MSWD of equivalence = 0.2). They yield a weighted mean $^{207}Pb/^{206}Pb$ date of $999.7 \pm 0.3/5.0$ Ma (MSWD = 0.2), a weighted mean $^{207}Pb/^{235}U$ date of $998.5 \pm 0.2/0.2/1.1$ Ma (MSWD = 0.4), and a weighted mean $^{206}Pb/^{238}U$ date of $997.9 \pm 0.2/0.3/1.3$ Ma (MSWD = 0.3).

3.9. Zircon z6266

z6266 is a zircon megacryst from Sri Lanka (Stern, 2001; Stern and Amelin, 2003) for which Stern and Amelin (2003) assigned a weighted mean $^{207}Pb/^{206}Pb$ date of 562.6 ± 0.4 Ma (MSWD = 1.2) and a weighted mean $^{206}Pb/^{238}U$ date of 559.0 ± 0.2 Ma (MSWD = 1.1). Five chemical-abraded and two air-abraded grains that we analyzed form a discordant cluster (MSWD of equivalence = 0.8). They yield a weighted mean $^{207}Pb/^{206}Pb$

date of 562.00 ± 0.50/4.59 Ma (MSWD = 0.9), a weighted mean $^{207}Pb/^{235}U$ date of 559.80 ± 0.13/0.18/0.76 Ma (MSWD = 1.0), and a weighted mean $^{206}Pb/^{238}U$ date of 559.27 ± 0.11/0.19/0.79 Ma (MSWD = 0.7).

3.10. North Mountain basalt (NMB-03-1)

The North Mountain basalt was erupted in association with the rifting of North America in the early Jurassic and is part of the Newark Supergroup, Nova Scotia, Canada (Hodych and Dunning, 1992). Pegmatitic lenses within the basalt contain abundant zircon which Hodych and Dunning (1992) assigned a $^{206}Pb/^{238}U$ date of 202 ± 1 Ma based on two multi-grain analyses. Ten air-abraded zircon grains (collected from the same locality) that we analyzed form a statistically significant cluster (MSWD of equivalence = 0.8). They yield a weighted mean $^{207}Pb/^{206}Pb$ date of 203.97 ± 0.45/4.32 Ma (MSWD = 0.9), a weighted mean $^{207}Pb/^{235}U$ date of 201.48 ± 0.05/0.07/0.32 Ma (MSWD 0.7), and a weighted mean $^{206}Pb/^{238}U$ date of 201.27 ± 0.03/0.06/0.27 Ma (MSWD = 0.7).

3.11. GA-1550 monzonite (RSES01-98)

The GA-1550 biotite, derived from Mount Dromedary complex, south of Narooma, New South Wales, Australia, is one of the few primary K–Ar standards for which an age has been determined based on a direct calibration of its $^{40}Ar^{*}$ concentration against a known volume of air. Three K–Ar age determinations or recalibrations have been published: 97.9 ± 1.8 (McDougall and Roksandic, 1974), 98.8 ± 1.0 (Renne et al., 1998b), and 98.5 ± 1.6 (Spell and McDougall, 2003) (decay constant uncertainties excluded). Sample RSES01-98 is a recollection of the monzonite from the original quarry that yielded GA-1550 (McDougall and Roksandic, 1974; Spell and McDougall, 2003).

Twenty zircons were analyzed, including three chemical-abraded grains, and all analyses except one gave $^{206}Pb/^{238}U$ dates of ca. 99.1 Ma. Although they define a clear cluster, the 19 analyses are not equivalent. In addition to Pb-loss and inheritance, intermediate daughter product disequilibria can explain scatter in the $^{207}Pb/^{235}U$ (i.e., z6, z10, z11, z12, z10.5, and z16) and $^{206}Pb/^{238}U$ (z5, z15, z17aa, and z18aa) ratios, and these possibilities for zircon discordance will be discussed in detail in the following section. While analytical inaccuracies could also create the observed scatter in the results, the consistency of the analyses from other samples in this study suggests otherwise. Regardless of the cause of the scatter, the 10 analyses that form a statistically significant cluster (MSWD of equivalence = 0.7) and are closest to concordia are likely to represent the crystallization age of the rock. The 10 equivalent analyses yield a weighted mean $^{207}Pb/^{206}Pb$ date of 102.14 ± 0.47/4.26 Ma (MSWD = 0.5), a weighted mean $^{207}Pb/^{235}U$ date of 99.24 ± 0.03/0.04/0.17 Ma (MSWD = 0.8), and a weighted mean $^{206}Pb/^{238}U$ date of 99.12 ± 0.02/0.03/0.14 Ma (MSWD = 1.0).

4. Discussion

4.1. Interpretation of systematic discordance of U–Pb data

Assigning high-precision absolute crystallization ages to the samples is complicated because the $^{207}Pb/^{206}Pb$ dates do not agree within internal error of the $^{206}Pb/^{238}U$ dates (Figs. 1 and 2). Explanations for the data include: (1) intermediate daughter product disequilibria, (2) Pb-loss, (3) systematic analytical inaccuracies, and (4) decay constant inaccuracies.

The incorporation of ^{231}Pa and ^{230}Th outside of secular equilibrium during mineral crystallization results in either an excess or deficiency of their respective daughter products, ^{207}Pb and ^{206}Pb, (Anczkiewicz et al., 2001; Mattinson, 1973; Mortensen et al., 1992; Parrish, 1990; Schärer, 1984). If this phenomenon were important in shifting mineral dates below concordia, as is observed in this study, it necessitates a preferential exclusion of Th or a preferential inclusion of Pa in the crystal lattice compared to the magma. Evaluating the magnitude of such effects is difficult because it requires some knowledge of the ratio of the Th/U (or Pa/U) in the crystal to the Th/U (or Pa/U) in the host magma. ^{230}Th disequilibrium is more easily dealt with in this case because there is a limit of −108 kyr in the $^{206}Pb/^{238}U$ date caused by Th deficiency (Parrish, 1990). Therefore, the potential effect of ^{230}Th disequilibrium is a strong function of the age of the sample compared to the amount of discordance observed. For example, in the youngest sample, RSES01-98, the discordance of the weighted mean dates is 2.96 ± 0.45% and with a maximum correction for ^{206}Pb deficiency, the discordance becomes 0.27 ± 0.47% and is concordant within errors. For the second youngest sample, the North Mountain Basalt, the discordance shifts from 1.32 ± 0.22 to 0.68 ± 0.22% discordant, which is significant but not enough to explain the discordance. The effect becomes increasingly insignificant, such that for the oldest sample, JCA-62-02, the discordance only shifts from 0.121 ± 0.023 to 0.117 ± 0.023%. ^{231}Pa excess is more difficult to quantify because there is no theoretical limit to its magnitude, very little is known about the distribution coefficient of Pa between minerals and magmas, and the oxidation state of the magma and therefore the valence of Pa may play a large role in its compatibility in zircon and xenotime. Qualitative arguments for compatibility of Pa into zircon show that in the tetravalent state, Pa^{4+} is likely to be less compatible that Zr^{4+}, and would cause a small deficiency in ^{207}Pb and therefore cannot explain our datasets (Barth et al., 1989; Mattinson, 1973; Schmitz and Bowring, 2001). In the pentavalent state, Pa^{5+} is likely to be more compatible in zircon and may be responsible for documented examples of excess ^{207}Pb (Anczkiewicz et al., 2001; Mattinson, 1973; Mortensen et al., 1992) and may also be the cause for subtle scatter in many U–Pb datasets (Amelin and Zaitsev, 2002). While we speculate that excess ^{207}Pb may be partially responsible for the observed scatter in $^{207}Pb/^{235}U$ dates in sample RSES01-98, we find it

exceedingly unlikely that it would affect each analyzed zircon from a sample equally and as a function of age such that older samples show systematically larger absolute offset. Such systematic discordance is likely derived from a systematic source.

Numerous studies have shown that U–Pb systematics in zircon are usually complicated by an obvious or subtle combination of multi-stage Pb-loss and inheritance, which results in discordant data (e.g., Corfu et al., 2003; Pidgeon and Aftalion, 1978; Wetherill, 1956). In fact, discordance is observed so frequently in zircons from both young and old igneous and metamorphic rocks such that seeking out concordant zircons based on geologic context is nearly impossible. However, nearly all processes that produce discordance are highly unlikely to affect all grains from a sample equally. In the case of Pb-loss, a common interpretation is that the upper intercept of a discordia or a weighted mean $^{207}Pb/^{206}Pb$ date (for samples with recent Pb-loss) is the best approximation of a crystallization age (see reviews in Davis et al., 2003; Ireland and Williams, 2003; Parrish and Noble, 2003). Either interpretation hinges on zircon discordance being a result of a single stage of Pb-loss and the observation that such open-system behavior is unlikely to affect every zircon from a population equally. Discordant data produced from a mixture of two or more domains of different ages are also unlikely to affect every zircon from a sample equally. Because our data consist of statistically equivalent, high-*n*, datasets from samples of various ages, neither open-system behavior nor inheritance is a viable explanation for the systematic discordance observed. Instead, these data suggest that such factors, if present, were eliminated through rigorous grain pre-treatment including air-abrasion and/or chemical-abrasion.

The most important sources of systematic experimental inaccuracies involve Pb mass fractionation and the calibration of the ^{205}Pb–^{233}U–^{235}U tracer solution. We are confident that Pb mass fractionation is accurate to within the quoted errors (±0.04%/a.m.u.), and a sensitivity test shows that reasonable changes in those values change all U–Pb and $^{207}Pb/^{206}Pb$ dates of a given sample, but do not significantly change the amount of discordance. The best way to address any inaccuracies in Pb mass fractionation for geochronology, which will become increasingly important in high-precision U–Pb geochronology, is through the use of a ^{202}Pb–^{205}Pb double spike (Todt et al., 1996).

The ^{205}Pb–^{233}U–^{235}U tracer solution used in this study was recently calibrated through a total of 11 experimental isotope dilution mixtures (see analytical details). We note that the new tracer calibration used in this study differs from previous calibrations, and a notable example is that the $^{206}Pb/^{238}U$ date from sample AS3 in this study differs from that of Schmitz et al. (2003) by ~0.25%, largely from differences in tracer calibration. Schmitz et al. (2003) suggest based on concordant zircon data from that study that the U decay constants need no revision, but note that because the magnitude of systematic uncertainties of the tracer calibration approaches that of the reported errors in the U decay constants, their ability to quantitatively evaluate the accuracy of the U decay constants is limited. The present tracer calibration is more precise than previous calibrations and we also believe it to be more accurate for several reasons: (1) decreased U blank in tracer calibration experiments through oxide analysis of U; (2) the isotopic composition of U in the tracer was determined by multiple methods including critical mixtures (Hofmann, 1971; Roddick et al., 1992) and standard isotope dilution with mass fractionation corrected by referencing multiple standard U solutions; (3) measurement of the Pb/U ratio in the tracer was conducted against three mixed U–Pb gravimetric solutions that were prepared in independent laboratories (see description in the analytical methods). The high level of internal agreement of the resulting Pb/U ratio of the tracer (2SE = 0.015%) ensures that any systematic errors that resulted from mixing, weighing, dilution, distribution, or the initial isotopic composition and concentrations of the gravimetric solutions were very small relative to the magnitude of observed discrepancies between U–Pb and $^{207}Pb/^{206}Pb$ dates.

Multiple recent ID-TIMS U–Pb studies from other laboratories with independent mixed Pb–U tracers also observe slight discordance in weighted mean clusters of zircons with $^{207}Pb/^{206}Pb$ dates that are older than $^{206}Pb/^{238}U$ dates by ~0.3–0.6%. Datasets acquired at the Royal Ontario Museum from samples Temora 1 (Black et al., 2003a), QGNG (Black et al., 2003b), R33 (Black et al., 2004), and z6266 (Stern and Amelin, 2003) all plot slightly below the concordia curve. Data from z6266 acquired at the Geological Survey of Canada show similar results (Stern and Amelin, 2003). We stress that continued high-precision analysis of zircon standards by multiple laboratories is the best way to provide an external check for tracer calibration and other resolvable analytical problems that result in interlaboratory variability.

Given that we rule out geological and analytical explanations for the discordance in our datasets, the only viable explanation for our data is that there is a systematic inaccuracy, albeit within the stated uncertainties, in the presently accepted values of the U decay constants.

4.2. Assessing inaccuracies of the U decay constants

The ^{238}U and ^{235}U decay constants are the most precisely known of those used in geochronology, with assigned 95% confidence interval uncertainties of 0.107 and 0.136%, respectively, based on the alpha-counting experiments of Jaffey et al. (1971). That study included four experiments on two separate batches of high-purity ^{238}U and two experiments on one batch of high-purity ^{235}U. All four experiments on ^{238}U produced results that agree within error and showed no indication of systematic errors or drift in the experiments. The ^{235}U experiments were more precise than the ^{238}U experiments, but were shown to have an unknown source of systematic drift over the course of the measurements, such that the two sequential

experiments did not agree within error. To account for this, Jaffey et al. (1971) multiplied the counting errors of the ^{235}U activity results by 1.5 and propagated those into the quoted errors for the study. Finally, Jaffey et al. (1971) concluded that if further systematic errors exist, they "will no more than double the quoted errors." Because of this, Mattinson (1987) suggested that the stated errors of the ^{238}U and ^{235}U decay constants should be inflated by a further 50% for realistic use in geochronology.

Because individual U–Pb analyses of zircons in this study approach the precision of the decay constants and weighted means of equivalent populations are well within those errors, it is possible to validate the accuracy of the Jaffey et al. (1971) counting experiments empirically and quantitatively (Begemann et al., 2001; Mattinson, 1994a,b, 2000). We believe that the analyses presented in this study, which consistently plot below the concordia curve (Fig. 1), are indicative of a systematic inaccuracy in one or both of the U decay constants. Mattinson (2000) reached a similar conclusion based on multigrain analyses of <200 Ma zircon that yield $^{207}Pb/^{206}Pb$ dates that are systematically older than the $^{206}Pb/^{238}U$ dates by 2 Myr (with uncertainties of <1 Myr). Based on the assumption that the ^{238}U decay constant is correct, Mattinson (2000) calculated a ^{235}U decay constant of 9.857×10^{-10} yr^{-1} that is within the error of the Jaffey et al. (1971) value but 0.09% higher than the mean value.

We are now in a better position to quantitatively evaluate the accuracy of the U decay constants using large datasets of single grains or grain fragments that span over three billion years. The discrepancy between $^{207}Pb/^{206}Pb$ and $^{206}Pb/^{238}U$ in our data is, in fact, identical within errors to that documented by Mattinson (2000) (Fig. 3), and if we make the assumption that the ^{238}U decay constant is correct, we calculate a ^{235}U decay constant of $9.8569 \pm 0.0017/0.0110 \times 10^{-10}$ yr^{-1} (without/with error of λ_{238}; Fig. 3). On the other hand, if we make the assumption that the ^{235}U decay constant is correct, we calculate a ^{238}U decay constant of $1.54993 \pm 0.00026/0.00219 \times 10^{-10}$ yr^{-1} (without/with error of λ_{235}; Fig. 3). Both numbers are within error of the Jaffey et al. (1971) values, but 0.09% different than the mean value. The most robust and precise calculation provided by our data, and the number that determines whether or not a datum is concordant, is the ratio between the ^{238}U and the ^{235}U decay constants (0.15738 ± 0.00003; Fig. 3), because it involves no assumption about the absolute values of either decay constant and therefore we need not propagate their errors. We should note that the

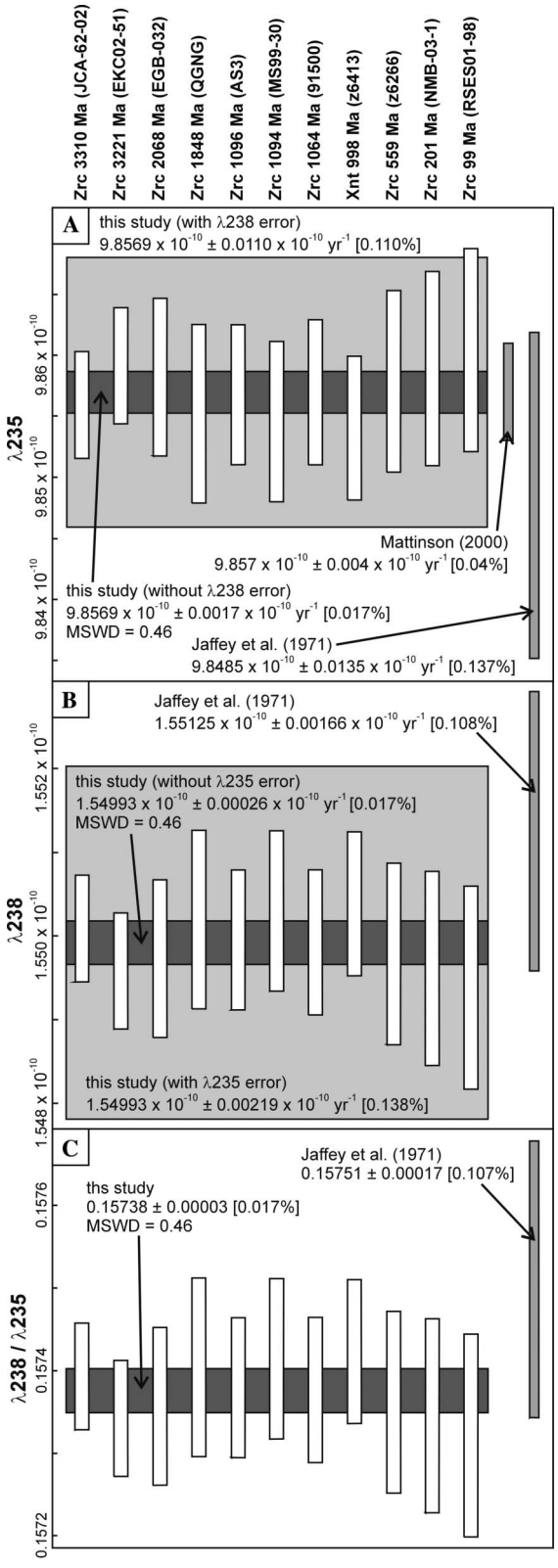

Fig. 3. U decay constants calculated from our U–Pb data (sample numbers shown across the top), compared against values of Jaffey et al. (1971) and Mattinson (2000) (the latter does not include errors in λ_{238}). (A) Calculated ^{235}U decay constant, assuming the value ^{238}U decay constant is correct. (B) Calculated ^{238}U decay constant, assuming the value ^{235}U decay constant is correct. (C) Calculated ratio of the U decay constants, making no assumptions about their absolute values. Errors are at the 95% confidence interval and are calculated using standard error-propagation techniques and by assuming concordance of weighted mean $^{206}Pb/^{238}U$ and $^{207}Pb/^{235}U$ ratios of statistically significant clusters and calculating the weighted mean decay constant values and errors. Decay constant errors of ^{235}U and ^{238}U from Jaffey et al. (1971) are propagated after weighted mean decay constants of ^{238}U and ^{235}U, respectively, are calculated.

equivalence of the different datasets as shown in Fig. 3 further supports the assertion that factors such as intermediate daughter product disequilibrium or Pb-loss are not likely to be an important cause for the discordance. The error in the calculated decay constants without incorporating uncertainties of the counting experiments from Jaffey et al. (1971) (but with tracer uncertainties) is 0.017%, but increases to 0.110 and 0.138% for the calculated ^{235}U and ^{238}U decay constants, respectively, with the systematic addition of those errors. Therefore, the precision of the ratio of the decay constants can be increased with additional U–Pb data, but the ultimate precision of either decay constant individually cannot be better than the error of the most precise counting experiment.

The thorough discussion of the potential errors and sources of those errors in Jaffey et al. (1971) suggests that if only one of the decay constants is inaccurate, it is most likely ^{235}U. For this reason, some workers have suggested recalibrating the ^{235}U decay constant to that of ^{238}U (e.g., Mattinson, 2000), with the goal of improving its accuracy and precision. Although this intercalibration reduces the uncertainty on the ^{235}U decay constant by ~20%, further refinement through intercalibration is limited by the precision of the ^{238}U decay constant. Therefore, we join others (Begemann et al., 2001; Schön et al., 2004) in suggesting that for the purposes of high-precision geochronology and the attainment of a highly robust, internally consistent geologic time-scale calibrated by multiple dating methods, the best way to address the issue of decay constant inaccuracies is to repeat the alpha-counting experiments of Jaffey et al. (1971). Without this, high-precision *intercomparative* geochronology from multiple dating methods beyond the 0.1% level is precluded.

Acceptance of inaccuracy in one or both of the U decay constants raises the question of which date(s) should be used to for establishing high-precision benchmarks in the geological time-scale. $^{206}Pb/^{238}U$, $^{207}Pb/^{235}U$, and $^{207}Pb/^{206}Pb$ cannot be compared accurately without propagating decay constant errors, and in fact, the concept of an "absolute age" is difficult to defend. For problems that calculate durations of events or depositional sequences, however, it is the relative differences in dates that are most crucial. In these cases, the most precise of the three systems is the best date to use, given the sample-specific caveats of Pb-loss and intermediate daughter product disequilibria.

4.3. Comparison of U–Pb dates with $^{40}Ar/^{39}Ar$ dates

Several recent studies have pointed out the systematic offset between U–Pb and $^{40}Ar/^{39}Ar$ dates (Chambers et al., 2005; Kamo et al., 2003; Min et al., 2000, 2001; Nomade et al., 2004; Renne, 2000; Renne et al., 1998a; Schmitz and Bowring, 2001). Table 2 and Fig. 4 summarize the data discussed in those papers, other pertinent data from the literature, and also the data from the four samples that we analyzed. The assumption underlying each of these comparisons, which is often discussed in the original studies, is that both the U–Pb dates and $^{40}Ar/^{39}Ar$ dates record the same geologic event (e.g., crystallization from a magma). Magma residence time in young plutonic and volcanic systems may invalidate that assumption and possibly affect the U–Pb data from the Fish Canyon Tuff (Reid and Coath, 2000; Reid et al., 1997; Schmitz and Bowring, 2001) and other young igneous rocks. Intermediate daughter product disequilibria in zircon are difficult to address but may be significant in U–Pb dates from rocks <100 Ma (see previous discussion). Problems associated with magma residence time and intermediate daughter product disequilibria are more easily overcome in older rocks, because their absolute effects likely become negligible as a percentage of the age and associated uncertainty. Another source of complication arises from the post-crystallization thermal histories of the rocks in question and the fact that the different phases analyzed for U–Pb and $^{40}Ar/^{39}Ar$ have different closure temperatures and are involved in a suite of different metamorphic reactions. For example, it is unclear whether currently published $^{40}Ar/^{39}Ar$, U–Pb, and Pb–Pb dates from the Bushveld Complex and the Acapulco meteorite represent cooling or metamorphic ages (Table 2, Figs. 4 and 5; Buick et al., 2001; Nomade et al., 2004; Renne, 2000), though (U–Th)/He data from the meteorite are consistent with rapid cooling (Min et al., 2003). The data from the Kaap Valley pluton are difficult to compare because of a complicated low-temperature thermal history and the potential for alteration in hornblende and apatite over three billion years (Layer et al., 1992; Schoene and Bowring, 2003). When comparing U–Pb and $^{40}Ar/^{39}Ar$ dates, these problems are heightened by potential inaccuracies in the U decay constants (discussed above) and also in comparing $^{40}Ar/^{39}Ar$ dates determined by total fusion and step-heating experiments (e.g., McDougall and Harrison, 1999). In many examples from the literature (Table 2, Fig. 4), certain geologic or laboratory biases may have been negligible for the goals of those studies, but may be important for the purposes of high-precision intercomparative geochronology. We choose to include all the available data in the following discussion to examine the problem as it exists now, with hopes that it will emphasize the importance of examining those concerns in future studies that compare U–Pb and $^{40}Ar/^{39}Ar$ data.

The intercalibration efforts cited from the literature and presented in this study have two important aspects in common: (1) mean $^{40}Ar/^{39}Ar$ dates are within internal errors or systematically younger than $^{207}Pb/^{206}Pb$, $^{207}Pb/^{235}U$, and $^{206}Pb/^{238}U$ dates (Table 2, Figs. 4 and 5), and (2) if external sources of error are included in the age estimates, dates from both isotopic schemes are statistically indistinguishable (with the exception of the Acapulco meteorite; Fig. 4). U–Pb data from this study suggest that inaccuracies in the U decay constants introduce a small bias between the two dating techniques, which will change as a function of age (Fig. 5A). Other important potential sources of bias include the decay constants and physical con-

Table 2
Summary of U-Pb and $^{40}Ar/^{39}Ar$ comparison from geologic samples

	$^{40}Ar/^{39}Ar$ date[a]					U-Pb date[c]					
	(Ma)	±[b]	Mineral	Reference	Interpretation	(Ma)	±[b]	Type	Reference	% difference[d]	±[b]
Fish Canyon	28.02	0.06	Sanidine	Renne et al. (1998b)	Timing of eruption	28.478	0.024	$^{206}Pb/^{238}U$	Schmitz and Bowring (2001)	1.62	0.23
	28.12	*0.08*	Sanidine	Spell and McDougall (2003)	Timing of eruption						
MAC-83 Tuff	24.25	0.10	Biotite	Villeneuve et al. (2000)	Timing of eruption	24.22	0.08	$^{207}Pb/^{235}U$	Villeneuve et al. (2000) *monazite*	−0.14	0.53
Rum complex	60.60	1.0	Phlogopite	Hamilton et al. (1998)	Timing of crystallization	60.53	0.08	$^{206}Pb/^{238}U$	Hamilton et al. (1998)	−0.21	1.67
Cuillin complex	58.10	1.2	Biotite	Hamilton et al. (1998)	Timing of crystallization	58.91	0.07	$^{206}Pb/^{238}U$	Hamilton et al. (1998)	1.34	2.11
Muck Tuff	61.54	0.19	Sanidine	Chambers et al. (2005)	Timing ot eruption	61.08	0.27	$^{206}Pb/^{238}U$	Chambers et al. (2005)	−0.75	0.53
GA1550 (K-Ar)	98.8	1.1	Biotite	Renne et al. (1998b)	Crystallization/cooling	102.14	0.47	$^{207}Pb/^{206}Pb$	This study	3.38	1.23
	98.5	1.6	Biotite	Spell and McDougall (2003)		99.12	0.02	$^{206}Pb/^{238}U$	This study	0.32	1.10
	97.9	1.8	Biotite	McDougall and Roksandic (1974)							
Siberian Traps	250.0	0.2	Sanidine	Renne and Basu (1991)	Timing of eruption	251.7	0.4	$^{206}Pb/^{238}U$	Kamo et al. (2003)	0.67	0.18
						251.1	0.3	$^{206}Pb/^{238}U$	Kamo et al. (2003)	0.43	0.14
						251.3	0.2	$^{206}Pb/^{238}U$	Kamo et al. (1996)	0.51	0.11
P-T boundary	249.9	0.2	Sanidine, plagioclase	Renne et al. (1995)	Bracket provided by eruption ages above and below the boundary	252.2	0.4	$^{206}Pb/^{238}U$	Mundil et al. (2004)	0.91	0.18
Deicke	449.8	2.3	Sanidine	Min et al. (2001)	Timing of eruption	454.5	0.5	$^{206}Pb/^{238}U$	Tucker (1992)	1.03	0.53
Millbrig	448.0	2.0	Sanidine	Min et al. (2001)	Timing of eruption	453.1	1.3	$^{206}Pb/^{238}U$	Tucker (1992)	1.13	0.54
Kinnekulle	454.8	2.0	Sanidine	Min et al. (2001)	Timing of eruption	456.9	1.8	U-Pb	Tucker and McKerrow (1995)	0.45	0.59
Bushveld Complex	2042.4	3.2	Biotite	Nomade et al. (2004)	Post-intrusion metasomatic growth	2058.9	0.8	$^{207}Pb/^{206}Pb$	Buick et al. (2001) *titanite metamorphic/cooling date*	0.81	0.16
Acapulco meteorite	4507	18	Plagioclase	Renne (2000)	Cooling date	4557	2	$^{207}Pb/^{206}Pb$	Göpel et al. (1992)	1.10	0.41
Palisade rhyolite	1088.4	3.6	Sanidine	Min et al. (2000)	Timing of eruption	1097.6	2.1	$^{207}Pb/^{206}Pb$	Min et al. (2000)	0.84	0.38
						1096.1	0.4	$^{207}Pb/^{206}Pb$	This study	0.71	0.33
						1094.2	0.2	$^{206}Pb/^{238}U$	This study	0.54	0.33
Eglab porphyry	2054.8	2.4	Hornblende	P. Renne, Pers. Comm.	Timing of eruption	2071.6	0.4	$^{207}Pb/^{206}Pb$	This study	0.81	0.12
						2067.5	0.7	$^{206}Pb/^{238}U$	This study	0.62	0.12
Kaap Valley pluton	3218.3	6.7	Hornblende	Layer et al. (1992)	Cooling date	3227	1	$^{206}Pb/^{238}Pb$	Kamo and Davis (1994)	0.27	0.21
						3227.2	0.2	$^{207}Pb/^{206}Pb$	This study	0.28	0.21
						3221.4	0.8	$^{206}Pb/^{238}U$	This study	0.10	0.21

[a] Dates not in italics are normalized to FCs = 28.02 using the GA1550/FCs calibration of Renne et al. (1998b). Kaap Valley pluton data were renormalized to FCs = 28.02 using the Hb3gr/FCs calibration of Renne (2000). Muck Tuff renormalized using FCs/Taylor Creek sanidine of Renne et al. (1998b). Date in italics is normalized using primary GA 1550 calibration and GA1550/FCs calibration of Spell and McDougall (2003). GA-1550 dates are K-Ar primary calibrations.

[b] Errors are at the 95% confidence interval and exclude errors for the age of GA1550, the GA1550/FCs calibration, and external errors.

[c] U-Pb dates are all interpreted to be zircon crystallization dates except for the Acapulco meteorite, which is a Pb-Pb isochron cooling date from phosphates, the sphene metamorphic cooling date from Buick et al. (2001) from the Bushveld complex, and the monazite date from Villeneuve et al. (2000).

[d] % difference is calculated relative to the uppermost $^{40}Ar/^{39}Ar$ or K-Ar date.

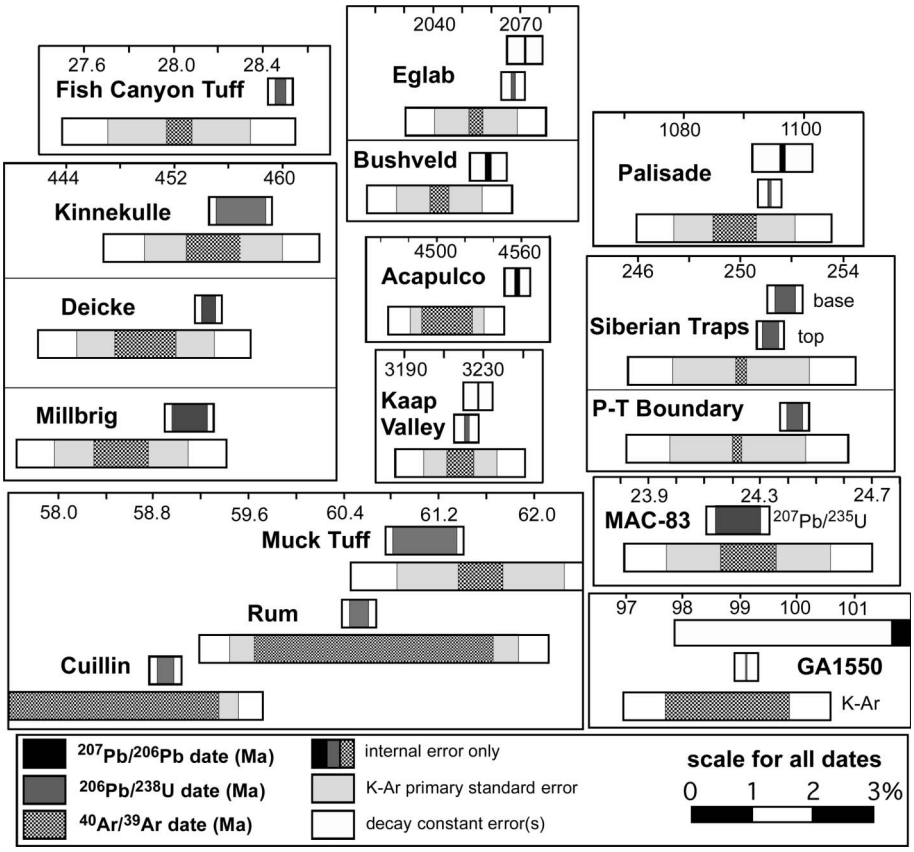

Fig. 4. Summary diagram for U–Pb and $^{40}Ar/^{39}Ar$ dates (in Ma). $^{40}Ar/^{39}Ar$ data are normalized to Fish Canyon sanidine = 28.02 Ma and the primary standard GA1550 Ar^*/K values of Renne et al. (1998b). Tracer calibration errors for data from this study are negligible at the shown scale and those from other studies are not reported. References are given in Table 2. Errors are at the 95% confidence level.

stants of ^{40}K, the K–Ar age calibration of primary standards, and the intercalibration of other $^{40}Ar/^{39}Ar$ secondary standards with primary standards. Fig. 5A shows the contribution of various sources of systematic errors in $^{40}Ar/^{39}Ar$ dates as a function of the age of the sample, calculated using the techniques of Karner and Renne (1998), Min et al. (2000), and Renne et al. (1998b). Plotted in Fig. 5B are the offsets between U–Pb and $^{40}Ar/^{39}Ar$ or K–Ar dates, which show that in samples <2 Ga, U–Pb and $^{40}Ar/^{39}Ar$ dates are indistinguishable if one ignores decay constant errors but includes the error of the primary K–Ar standard (the data are relative to GA1550 of Renne et al., 1998b and the Fish Canyon sanidine (FCs) at 28.02 Ma, and using the ^{40}K decay constants of Steiger and Jäger, 1977), in that all of the data plot within the extent of the GA1550 primary standard uncertainties (black dashed line in Fig. 5B is the 2σ upper bounds of that calibration). The offsets between U–Pb and $^{40}Ar/^{39}Ar$ dates for the Bushveld Complex, the Eglab porphyry, and the Acapulco meteorite are likely to be outside the error-bounds introduced by the Ar^*/K calibration of GA1550 from Renne et al. (1998b), and therefore some of the bias must lie in the ^{40}K decay constant or physical constants (Fig. 5B). Fig. 5B also shows the effect on $^{40}Ar/^{39}Ar$ dates if the data are re-normalized to the GA1550 K–Ar date and GA1550/FCs values of Spell and McDougall (2003); note that the reported errors on the K–Ar date are ~60% larger than those from Renne et al. (1998b).

Min et al. (2000) critically evaluated the selection criteria for the ^{40}K decay constants and physical constants (and associated errors) used in geochronology (Beckinsale and Gale, 1969), and concluded that the values suggested in Steiger and Jäger (1977) need to be revised. They recommended new values that more closely coincide with those from the nuclear physics and chemistry literature (Audi et al., 1997; Endt and Van der Leun, 1973) and indicated that larger associated errors are more realistic. Min et al. (2000) and Renne (2000) show that using the new recommended values, the bias between $^{207}Pb/^{206}Pb$ and $^{40}Ar/^{39}Ar$ dates for the Palisade rhyolite and Acapulco meteorite disappears (black solid curve in Fig. 5B; includes new values for the ^{40}K total decay constant, the branching ratio of the ^{40}K decay, and the $^{40}K/K$ value; we also fix the value of GA1550 to our $^{206}Pb/^{238}U$ date). Kwon et al. (2002) use a statistical regression approach to solve for the values of the total decay constant of ^{40}K and the age of the FCs (holding other variables constant), using a subset of data from the literature for which U–Pb or historical dates are available (gray solid curve in Fig. 5B; FCs = 28.269 Ma and λ_{40} less than Steiger and Jäger, 1977 by ~1.22%). Finally, different combinations of variations of the primary K–Ar standard, primary standard/secondary standard intercalibration, and decay

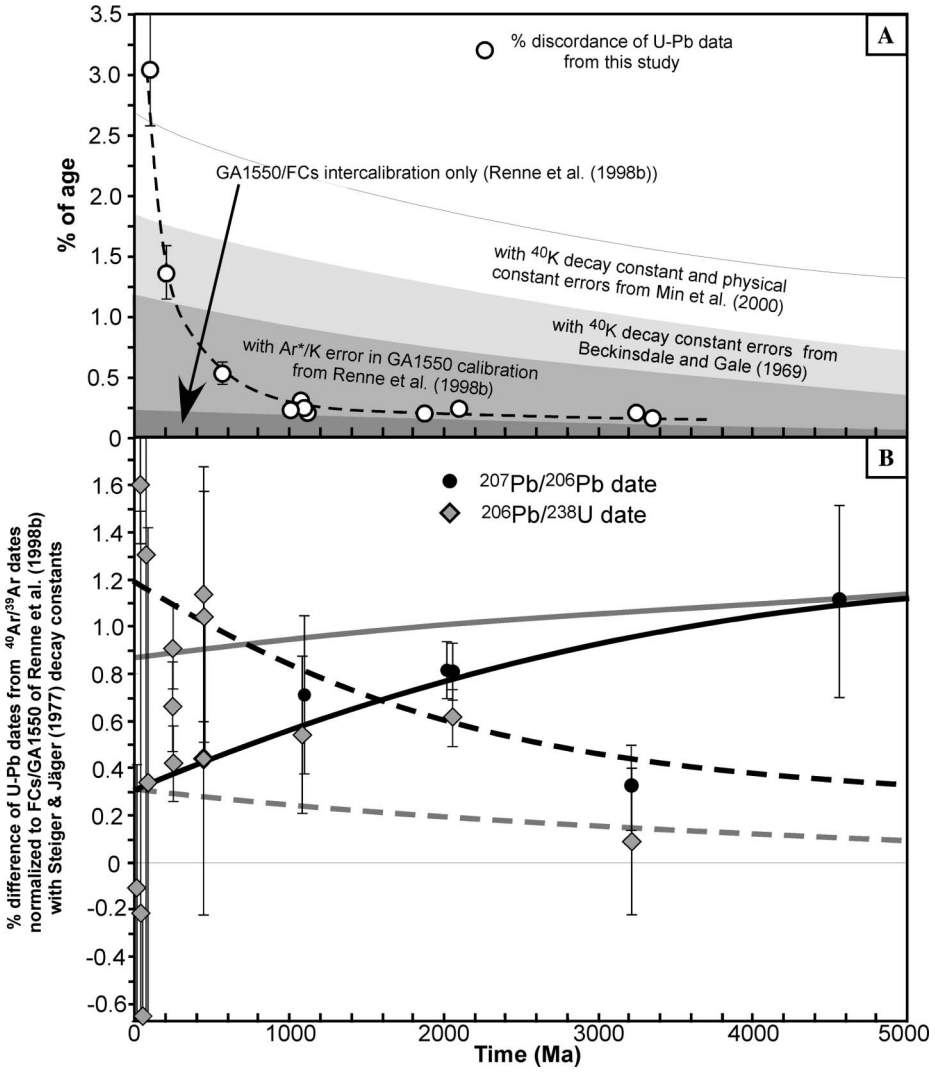

Fig. 5. Sensitivity analysis of systematic errors used in ^{40}Ar/^{39}Ar dates. The *Y*-axis in both diagrams is the % of the age, and the curves and U–Pb data in (B) are plotted as % offset from ^{40}Ar/^{39}Ar data in Table 2 and Fig. 4. (A) The magnitude of systematic errors from various sources in calculated ^{40}Ar/^{39}Ar dates as a function of age. Also plotted is the % discordance of the weighted mean dates of U–Pb data from this study. (B) The effects of varying parameters important in calculating ^{40}Ar/^{39}Ar dates. Curves are plotted as % difference from ^{40}Ar/^{39}Ar dates calculated using FCs = 28.02 Ma and the primary standard GA1550 Ar*/K values of Renne et al. (1998b). Black solid curve: effect of using the ^{40}K decay constants and physical constants (including ^{40}K/K) recommended by Min et al. (2000) and fixing the GA1550 age to our ^{206}Pb/^{238}U date. Gray solid curve: effect of using the age of the FCs and the ^{40}K decay constant of Kwon et al. (2002). Black dashed curve: effect of increasing the age of the K–Ar primary standard to its maximum error-bounds. Gray dashed curve: using the GA1550 Ar*/K and GA1550/FCs data from Spell and McDougall (2003), without showing the error-bounds, which are ~60% larger than those in the Renne et al. (1998b) calibration. Errors are at the 95% confidence level.

constant and physical constant uncertainties are able to produce similar offsets of U–Pb and ^{40}Ar/^{39}Ar dates, implying that there is no unique solution to this problem if one accounts for all the available variables from first principles. For geochronology, however, this final point is unimportant because if some combination of those variables produces accurate dates, then our purposes are served. Several aspects of Fig. 5 suggest that U–Pb and ^{40}Ar/^{39}Ar intercalibration is best done with older samples, if additional fresh samples can be obtained: (1) systematic errors in ^{40}Ar/^{39}Ar dates decrease as a percentage of age (Fig. 5A), and (2) the choice of primary standard in ^{40}Ar/^{39}Ar dating is less important for older samples (Fig. 5B).

High-precision intercalibration between ^{40}Ar/^{39}Ar and U–Pb data is precluded with the current dataset, as the large errors and absolute scatter in the offset between the two dating schemes suggest that the bias between those data is not created by systematic errors alone (Fig. 5). The scatter may arise from unexplored open-system behavior in either method or from interlaboratory variability. This observation highlights the importance of generating ^{40}Ar/^{39}Ar and U–Pb data from the same rocks from multiple laboratories and over a wide range of geologic time, such that systematic interlaboratory errors and geologic complexities can be distinguished from inaccuracies in the U and ^{40}K decay constants and physical constants.

5. Conclusions

High-precision statistically equivalent U–Pb datasets from this study systematically plot below the mean value of concordia, but within its reported errors. We believe this is indicative of inaccuracies in one or both of the mean values of the U decay constants and concur with previous literature that the bias likely resides in the currently used decay constant value for ^{235}U. Using U–Pb data alone, we recalculate the *ratio* of the decay constants with very high precision ($\pm\sim0.02\%$). Recalibrating the ^{235}U decay constant against that of ^{238}U can increase the precision of the former (from 0.14 to 0.11%), but a further increase in precision can only be accomplished through additional alpha-counting experiments (Begemann et al., 2001; Mattinson, 1994a,b, 2000).

Given tangible uncertainty in the U decay constants, comparison of $^{207}Pb/^{206}Pb$, $^{207}Pb/^{235}U$, and $^{206}Pb/^{238}U$ dates cannot be done accurately without incorporating decay constant errors. High-precision relative chronology within any one system need not incorporate decay constant errors, and the most appropriate system to use depends on which is the most precise and accurate. The accuracy of a given system for a specific sample depends on the importance of open-system behavior such as Pb-loss and intermediate daughter product disequilibria.

We compared U–Pb, $^{40}Ar/^{39}Ar$, and K–Ar dates from samples spanning a wide range of geologic time. Although external sources of error are too large to statistically distinguish between high-precision U–Pb and $^{40}Ar/^{39}Ar$ dates from any one sample, K–Ar and $^{40}Ar/^{39}Ar$ dates are systematically younger or within internal error of U–Pb dates, which is unlikely to be explained by geologic phenomena alone. However, these data do not form a trend that can be explained by only systematic errors, suggesting that interlaboratory biases or geologic complications are important in some or all of the samples examined.

High-precision intercalibration between the U–Pb and $^{40}Ar/^{39}Ar$ geochronology is hampered until (1) further experiments are carried out on determination of the U decay constants and (2) more datasets are generated from which we can compare and contrast data from a wide range of geologic time generated in a large number of laboratories. This must include the selection, documentation, and distribution of high quality accessory minerals to all laboratories involved in high-precision geochronology.

Studies that rely on the determination or tuning of decay constants for other chronometers such as Re–Os (Chen et al., 2002) and Lu–Hf (Scherer et al., 2001; Söderlund et al., 2004) by comparison to the U–Pb system must incorporate the effects resulting from uncertainty in the U decay constants.

Acknowledgments

This manuscript was greatly improved by reviews from J. Mattinson, R. Parrish, and J. Lee. Comments made on an early version of the manuscript by K. Hodges are much appreciated. This work was supported in part by NSF Grant EAR 0451802 (The EARTHTIME Network: Developing an infrastructure for high-resolution calibration of Earth History) to S. Bowring. Additional support was provided to B. Schoene by a subaward from NSF Grant EAR 031521 (CHRONOS to C. Cervato). We also thank C. Allen for providing zircon separates from GA-1550, N. Rayner for xenotime z6413, and S. Kamo for zircons QGNG and z6266.

Associate editor: Yuri Amelin

References

Amelin, Y., Zaitsev, A.N., 2002. Precise geochronology of phoscorites and carbonatites: the critical role of U-series disequilibrium in age interpretations. *Geochim. Cosmochim. Acta* **66** (13), 2399–2419.

Anczkiewicz, R., Oberli, F., Burg, J.P., Villa, I.M., Gunther, D., Meier, M., 2001. Timing of normal faulting along the Indus Suture in Pakistan Himalaya and a case of major $^{231}Pa/^{235}U$ initial disequilibrium in zircon. *Earth Planet. Sci. Lett.* **191**, 101–114.

Audi, G., Bersillon, O., Blanchot, J., Wapstra, A.H., 1997. The NUBASE evaluation of nuclear and decay properties. *Nucl. Phys.* **A624**, 1–124.

Barth, S., Oberli, F., Meier, M., 1989. U–Th–Pb systematics of morphologically characterized zircon and allanite: a high-resolution isotopic study of the Alpine Rensen pluton (northern Italy). *Earth Planet. Sci. Lett.* **95**, 235–254.

Beckinsale, R.D., Gale, N.H., 1969. A reappraisal of the decay constants and branching ratio of ^{40}K. *Earth Planet. Sci. Lett.* **6**, 289–294.

Begemann, F., Ludwig, K.R., Lugmair, G.W., Min, K., Nyquist, L.E., Patchett, P.J., Renne, P.R., Shih, C.-Y., Villa, I.M., Walker, R.J., 2001. Call for an improved set of decay constants for geochronological use. *Geochem. Cosmochim. Acta* **65** (1), 111–121.

Black, L.P., Kamo, S.L., Allen, C.M., Aleinikoff, J.N., Davis, D.W., Korsch, R.J., Foudoulis, C., 2003a. TEMORA 1: a new zircon standard for Phanerozoic U–Pb geochronology. *Chem. Geol.* **200**, 155–170.

Black, L.P., Kamo, S.L., Williams, I.S., Mundil, R., Davis, D.A., Korsch, R.J., Foudoulis, C., 2003b. The application of SHRIMP to Phanerozoic geochronology; a critical appraisal of four zircon standards. *Chem. Geol.* **200**, 171–188.

Black, L.P., Kamo, S.L., Allen, C.M., Davis, D.W., Aleinikoff, J.N., Valley, J.W., Mundil, R., Campbell, I.H., Korsch, R.J., WIlliams, I.S., Foudoulis, C., 2004. Improved $^{206}Pb/^{238}U$ microprobe geochronology by the monitoring of a trace-element-related matrix effect; SHRIMP, ID-TIMS, ELA-ICP-MS and oxygen isotope documentation for a series of zircon standards. *Chem. Geol.* **205**, 115–140.

Buick, I.S., Maas, R., Gibson, R., 2001. Precise U–Pb titanite age constraints on the emplacement of the Bushveld Complex, South Africa. *J. Geol. Soc. Lond.* **158**, 3–6.

Chamberlain, K.R., Bowring, S.A., 2000. Apatite-feldspar U–Pb thermochronometer: a reliable mid-range ($\sim$450 °C), diffusion controlled system. *Chem. Geol.* **172**, 173–200.

Chambers, L.M., Pringle, M.S., Parrish, R.R., 2005. Rapid formation of the Small Isles Tertiary centre constrained by precise $^{40}Ar/^{39}Ar$ and U–Pb ages. *Lithos* **79**, 367–384.

Chen, J.H., Papanastassiou, D.A., Wasserburg, G.J., 2002. Re–Os and Pd–Ag systematics in Group IIIAB irons and in pallasites. *Geochim. Cosmochim. Acta* **66** (21), 3793–3810.

Cherniak, D.J., 1993. Lead diffusion in titanite and preliminary results on the effects of radiation damage on Pb transport. *Chem. Geol.* **110**, 177–194.

Cherniak, D.J., Lanford, W.A., Ryerson, F.J., 1991. Lead diffusion in apatite and zircon using ion implantation and Rutherford Backscattering techniques. *Geochem. Cosmochim. Acta* **55**, 1663–1673.

Corfu, F., Hanchar, J.M., Hoskin, P.W.O., Kinny, P., 2003. Atlas of zircon textures. In: Hanchar, J.M., Hoskin, P.W.O. (Eds.), *Zircon*, vol. 53. Mineralogical Society of America, pp. 468–500.

Corfu, F., Stone, D., 1998. The significance of titanite and apatite U–Pb ages: constraints for the post-magmatic thermal-hydrothermal evolution of a batholithic complex, Berens River area, northwestern Superior Province, Canada. *Geochim. Cosmochim. Acta* **62** (17), 2979–2995.

Davis, D.W., Green, J.C., 1997. Geochronology of the North American Midcontinent rift in western Lake Superior and implications for its geodynamic evolution. *Can. J. Earth Sci.* **34**, 476–488.

Davis, D.W., Williams, I.S., Krogh, T.E., 2003. Historical development of zircon geochronology. In: Hanchar, J.M., Hoskin, P.W.O. (Eds.), *Zircon*, vol. 53. Mineralogical Society of America, pp. 145–181.

Endt, P.M., Van der Leun, C., 1973. Energy levels of A = 21–44 nuclei (V). *Nucl. Phys.* **A214**, 1–625.

Frost, B.R., Chamberlain, K.R., Schumacher, J.C., 2000. Sphene (titanite): phase relations and role as a geochronometer. *Chem. Geol.* **172**, 131–148.

Gerstenberger, H., Haase, G., 1997. A highly effective emitter substance for mass spectrometric Pb isotope ratio determinations. *Chem. Geol.* **136**, 309–312.

Göpel, C., Manhés, G., Allégre, C., 1992. U–Pb study of the Acapulco meteorite. *Meteoritics* **27**, 226.

Green, J.C., 1977. Keweenawan plateau volcanism in the Lake Superior region. In: Baragar, W.R.A., Coleman, L.C., Hall, J.M. (Eds.), *Volcanic Regimes in Canada*, vol. 16. Geological Association of Canada, pp. 407–422, Special Paper.

Green, J.C., Fitz III, T.J., 1993. Extensive felsic lavas and rheoignimbrites in the Keweenawan Midcontinent Rift plateau volcanics, Minnesota: petrographic and field recognition. *J. Volcanol. Geothermal Res.* **54**, 177–196.

Hamilton, M.A., Pearson, D.G., Thompson, R.N., Kelley, S.P., Emeleus, C.H., 1998. Rapid eruption of Skye lavas inferred from precise U–Pb and Ar–Ar dating of the Rum and Cuillin plutonic complexes. *Nature* **394**, 260–263.

Hewitt, D.F., 1953. Geology of the Brudenell-Raglan Area. *Annual report of the Ontario Department of Mines* **62** (Part 5), 85–86.

Hodych, J.P., Dunning, G.R., 1992. Did the Manicouagan impact trigger end-of-Triassic mass extinction? *Geology* **20**, 21–54.

Hofmann, A., 1971. Fractionation corrections for mixed-isotope spikes of Sr, K, and Pb. *Earth Planet. Sci. Lett.* **10**, 397–402.

Ireland, T.R., Williams, I.S., 2003. Considerations in zircon geochronology by SIMS. In: Hanchar, J.M., Hoskin, P.W.O. (Eds.), *Zircon*, vol. 53. Mineralogical Society of America, pp. 215–241.

Jaffey, A.H., Flynn, K.F., Glendenin, L.E., Bentley, W.C., Essling, A.M., 1971. Precision measurement of half-lives and specific activities of ^{235}U and ^{238}U. *Phys. Rev.* **C4**, 1889–1906.

Kamo, S.L., Czamanske, G.K., Krogh, T.E., 1996. A minimum U–Pb age for Siberian flood-basalt volcanism. *Geochim. Cosmochim. Acta* **60**, 3505–3511.

Kamo, S., Czamanske, G.K., Amelin, Y., Fedorenko, V.A., Davis, D.W., Trofimov, V.R., 2003. Rapid eruption of Siberian flood-volcanic rocks and evidence for coincidence with the Permian-Triassic boundary and mass extinction at 251 Ma. *Earth Planet. Sci. Lett.* **214**, 75–91.

Kamo, S., Davis, D.W., 1994. Reassessment of Archean crustal development in the Barberton Mountain Land, South Africa, based on U–Pb dating. *Tectonics* **13** (1), 167–192.

Karner, D.B., Renne, P.R., 1998. ^{40}Ar/^{39}Ar geochronology of Roman volcanic province tephra in the Tiber River valley: age calibration of middle Pleistocene sea-level changes. *GSA Bull.* **110** (6), 740–747.

Krogh, T.E., 1973. A low contamination method for hydrothermal decomposition of zircon and extraction of U and Pb for isotopic age determination. *Geochim. Cosmochim. Acta* **37**, 485–494.

Krogh, T.E., 1982. Improved accuracy of U–Pb zircon ages by the creation of more concordant systems using an air abrasion technique. *Geochim. Cosmochim. Acta* **46**, 637–649.

Kwon, J., Min, K., Bickel, P.J., Renne, P.R., 2002. Statistical methods for jointly estimating the decay constant of ^{40}K and the age of a dating standard. *Math. Geol.* **34** (4), 457–474.

Layer, P.W., Kröner, A., York, D., 1992. Pre-3000 Ma thermal history of the Archean Kaap Valley pluton, South Africa. *Geology* **20**, 717–720.

Ludwig, K.R., 1980. Calculation of uncertainties of U–Pb isotope data. *Earth Planet. Sci. Lett.* **46**, 212–220.

Ludwig, K.R., 1991. Isoplot—a plotting and regression program for radiogenic isotope data. *USGS Open-File report* **91-445**.

Ludwig, K.R., 1998. On the treatment of concordant uranium–lead ages. *Geochim. Cosmochim. Acta* **62** (4), 665–676.

Ludwig, K.R., 2000. Decay constant errors in U–Pb concordia-intercept ages. *Chem. Geol.* **166**, 315–318.

Mattinson, J.M., 1973. Anomalous isotopic composition of lead in young zircons. *Carnegie Inst. Yearbook* **72**, 613–616.

Mattinson, J.M., 1987. U–Pb ages of zircons: a basic examination of error propagation. *Chem. Geol.* **66**, 151–162.

Mattinson, J.M., 1994a. Real and apparent concordance and discordance in the U–Pb systematics of zircons: limitations of "high-precision" U/Pb and Pb/Pb ages. *Eos* **75**, 691.

Mattinson, J.M., 1994. Uranium decay constant uncertainties and their implications for high-resolution U–Pb geochronology. *GSA Abst. Prog.* **77** A221.

Mattinson, J.M., 2000. Revising the "gold standard"—the uranium decay constants of Jaffey et al., 1971. *Eos Trans. AGU, Spring Meet. Suppl., Abstract V61A-02*.

Mattinson, J.M., 2003. CA (chemical abrasion)-TIMS: high-resolution U–Pb zircon geochronology combining high-temperature annealing of radiation damage and multi-step partial dissolution analysis. *Eos Trans. AGU, Fall Meet. Suppl., Abstract V22E-06*.

Mattinson, J.M., 2005. Zircon U–Pb chemical-abrasion (CA-TIMS) method: combined annealing and multi-step dissolution analysis for improved precision and accuracy of zircon ages. *Chem. Geol.* **220** (1–2), 47–56.

McDougall, I., Harrison, T.M., 1999. *Geochronology and Thermochronology by the ^{40}Ar/^{39}Ar Method*. Oxford University Press, Oxford.

McDougall, I., Roksandic, Z., 1974. Total fusion ^{40}Ar/^{39}Ar ages using HIFAR reactor. *J. Geol. Soc. Aust.* **21**, 81–89.

Min, K., Farley, K.A., Renne, P.R., Marti, K., 2003. Single grain (U–Th)/He ages from phosphates in Acapulco meteorite and implications for thermal history. *Earth Planet. Sci. Lett.* **209**, 323–336.

Min, K., Mundil, R., Renne, P.R., Ludwig, K.R., 2000. A test for systematic errors in ^{40}Ar/^{39}Ar geochronology through comparison with U–Pb analysis of a 1.1 Ga rhyolite. *Geochim. Cosmochim. Acta* **64**, 73–98.

Min, K., Renne, P.R., Huff, W.D., 2001. ^{40}Ar/^{39}Ar dating of Ordovician K-bentonites in Laurentia and Baltoscandia. *Earth Planet. Sci. Lett.* **185**, 121–134.

Mortensen, J.K., Roddick, J.C., Parrish, R.R., 1992. Evidence for high levels of unsupported radiogenic ^{207}Pb in zircon from a granitic pegmatite: implications for interpretation of discordant U–Pb data. *EOS, Trans. Am. Geophys. Union* **73**, 370.

Mundil, R., Ludwig, K.R., Metcalfe, I., Renne, P.R., 2004. Age and timing of the Permian mass extinctions: U/Pb dating of closed-system zircons. *Science* **305**, 1760–1763.

Nomade, S., Renne, P.R., Merkle, R.K.W., 2004. ^{40}Ar/^{39}Ar age constraints on ore deposition and cooling of the Bushveld Complex, South Africa. *J. Geol. Soc. Lond.* **161**, 411–420.

Paces, J.B., Miller, J.D.J., 1993. Precise U–Pb ages of Duluth Complex and related mafic intrusions, northeastern Minnesota: geochronological insights to physical, petrogenetic, paleomagnetic, and tectonomagmatic processes associated with the 1.1 Ga Midcontinent Rift System. *J. Geophys. Res.* **98**, 13997–14013.

Paquette, J.-L., Pin, C., 2001. A new miniaturized extraction chromatography method for precise U–Pb zircon geochronology. *Chem. Geol.* **176** (1–4), 311–319.

Parrish, R.R., 1990. U–Pb dating of monazite and its application to geological problems. *Can. J. Earth Sci.* **27**, 1431–1450.

Parrish, R.R., Noble, S.R., 2003. Zircon U–Th–Pb geochronology by isotope dilution—thermal ionization mass spectrometry (ID-TIMS). In: Hanchar, J.M., Hoskin, P.W.O. (Eds.), *Zircon*, vol. 53. Mineralogical Society of America, pp. 183–213.

Peucat, J.-J., Capdevila, R., Drareni, A., Mahdjoub, Y., Kahoui, M., 2005. The Eglab massif in the West African Craton (Algeria), an original segment of the Eburnean orogenic belt: petrology, geochemistry and geochronology. *Precambrian Res.* **136**, 309–352.

Pidgeon, R.T., Aftalion, M., 1978. Cogenetic and inherited zircon U–Pb systems in granites: Palaeozoic granites of Scotland and England. In: Bowes, D.R., Leake, B.E. (Eds.), *Geological Journal Special Issue No. 10*. Seel House Press.

Reid, M.R., Coath, C.D., 2000. In situ U–Pb ages of zircons from the Bishop Tuff: no evidence for long crystal residence times. *Geology* **28**, 443–446.

Reid, M.R., Coath, C.D., Harrison, T.M., McKeegan, K.M., 1997. Prolonged residence times for the youngest rhyolites associated with Long Valley caldera: ion microprobe dating of young zircons. *Earth Planet. Sci. Lett.* **150**, 27–38.

Renne, P.R., 2000. $^{40}Ar/^{39}Ar$ age of plagioclase from Acapulco meteorite and the problem of systematic errors in cosmochronology. *Earth Planet. Sci. Lett.* **175**, 13–26.

Renne, P.R., Basu, A.R., 1991. Rapid eruption of the Siberian Traps flood basalts at the Permo-Triassic boundary. *Science* **253**, 176–179.

Renne, P.R., Karner, D.B., Ludwig, K.R., 1998a. Absolute ages aren't exactly. *Science* **282**, 1840–1841.

Renne, P.R., Swisher, C.C., Deino, A.L., Karner, D.B., Owens, T.L., DePaolo, D.J., 1998b. Intercalibration of standards, absolute ages and uncertainties in $^{40}Ar/^{39}Ar$ dating. *Chem. Geol.* **145**, 117–152.

Renne, P.R., Zichao, Z., Richards, M.A., Black, M.T., Basu, A.R., 1995. Synchrony and causal relations between Permian-Triassic boundary crises and Siberian flood volcanism. *Science* **269**, 1413–1416.

Roddick, J.C., Sullivan, R.W., Dudäs, F.O., 1992. Precise calibration of Nd tracer isotopic compositions for Sm-Nd studies. *Chem. Geol.* **97**, 1–8.

Schärer, U., 1984. The effect of initial ^{230}Th disequilibrium on young U–Pb ages: the Makalu case, Himalaya. *Earth Planet. Sci. Lett.* **67**, 191–204.

Scherer, E., Münker, C., Mezger, K., 2001. Calibration of the Lutetium-Hafnium clock. *Science* **293**, 683–687.

Schmitz, M.D., Bowring, S.A., 2001. U–Pb zircon and titanite sytematics of the Fish Canyon Tuff: an assessment of high-precision U–Pb geochronology and its application to young volcanic rocks. *Geochim. Cosmochim. Acta* **65** (15), 2571–2587.

Schmitz, M.D., Bowring, S.A., Ireland, T.R., 2003. Evaluation of Duluth Complex anorthositic series (AS3) zircon as a U–Pb geochronological standard: new high-precision isotope dilution thermal ionization mass spectrometry results. *Geochim. Cosmochim. Acta* **67** (19), 3665–3672.

Schoene, B., Bowring, S.A., 2003. U–Pb apatite and sphene thermochronology documenting mid-crustal temperature gradients during Archean lithospheric stabilization, Kaapvaal craton, southern Africa. *GSA Abst. Prog.* **35** (6), 594.

Schön, R., Winkler, G., Kutschera, W., 2004. A critical review of experimental data for the half-lives of the uranium isotopes ^{238}U and ^{235}U. *Appl. Radiat. Isotopes* **60**, 263–273.

Söderlund, U., Patchett, P.J., Vervoort, J.D., Isachsen, C.E., 2004. The ^{176}Lu decay constant determined by Lu–Hf and U–Pb isotope systematics of Precambrian mafic intrusions. *Earth Planet. Sci. Lett.* **219**, 311–324.

Spell, T.L., McDougall, I., 2003. Characterization and calibration of $^{40}Ar/^{39}Ar$ dating standards. *Chem. Geol.* **198**, 189–211.

Steiger, R.H., Jäger, E., 1977. Subcommission on Geochronology: convention on the use of decay constants in geo- and cosmochronology. *Earth Planet. Sci. Lett.* **36**, 359–362.

Stern, R.A., 2001. A new isotopic and trace element standard for the ion microprobe: preliminary TIMS U–Pb and electron microprobe data, current research. *Radiogenic Age and Isotopic Studies: Report 4*. Geological Survey of Canada, Ottawa, Canada.

Stern, R.A., Amelin, Y., 2003. Assessment of errors in SIMS zircon U–Pb geochronology using a natural zircon standard and NIST SRM 610 glass. *Chem. Geol.* **197**, 111–142.

Stern, R.A., Rayner, N., 2003. Ages of several xenotime megacrysts by ID-TIMS: potential reference materials for ion microprobe U–Pb geochronology. *Radiogenic Age and Isotopic Studies: Report 16*. Geological Survey of Canada, vol. Current Research 2003-F1, p. 7.

Todt, W., Cliff, R.A., Hanser, A., Hofmann, A.W., Evaluation of a ^{202}Pb–^{205}Pb double spike for high-precision lead isotope analysis. *AGU Geophysical Monograph*, vol. 95, *Earth Processes: Reading the isotopic Code*, pp. 29–37.

Tucker, R.D., 1992. U–Pb dating of plinian-eruption ashfalls by the isotopic dilution method: a reliable and precise tool for time-scale calibration and biostratigraphic correlation. *Geol. Soc. Am. Abst. Prog.* **24**, A198.

Tucker, R.D., McKerrow, W.S., 1995. Early Paleozoic chronology: a review in light of new U–Pb zircon ages from Newfoundland and Britain. *Can. J. Earth Sci.* **32**, 368–379.

Villeneuve, M., Sandeman, H.A., Davis, W.J., 2000. A method for intercalibration of U–Th–Pb and ^{40}Ar–^{39}Ar ages in the Phanerozoic. *Geochim. Cosmochim. Acta* **64** (23), 4017–4030.

Wetherill, G.W., 1956. Discordant uranium-lead ages. *Trans. Am. Geophys. Union* **37**, 320–326.

Wiedenbeck, M., Allé, P., Corfu, F., Griffin, W.L., Meier, M., Oberli, F., Von Quadt, A., Roddick, J.C., Spiegel, W., 1995. Three natural zircon standards for U–Th–Pb, Lu–Hf, trace element and REE analyses. *Geostand. Newslett.* **19**, 1–23.

York, D., 1966. Least-squares fitting of a straight line. *Can. J. Phys.* **44**, 1079–1086.

York, D., 1967. The best isochron. *Earth Planet. Sci. Lett.* **2**, 479–482.

Zartman, R.E., 1964. A geochronologic study of the Long Grove Pluton from the Llano uplift, Texas. *J. Petrol.* **5** (3), 359–408.